NASA CR134980

THE DESIGN OF AIRCRAFT BRAKE SYSTEMS, EMPLOYING COOLING TO INCREASE BRAKE LIFE

Robert P. Scaringe

Ting-Long Ho

Marshall B. Peterson

TRIBOLOGY LABORATORY

DEPARTMENT OF MECHANICAL ENGINEERING,

AERONAUTICAL ENGINEERING & MECHANICS

RENSSELAER POLYTECHNIC INSTITUTE

TROY, NEW YORK 12181

October 1975

Prepared for

AEROSPACE SAFETY RESEARCH AND DATA INSTITUTE

NATIONAL AERONAUTICS AND SPACE ADMINISTRATION

LEWIS RESEARCH CENTER

CLEVELAND, OHIO 44135

Under

NASA Grant NGR 33-018-152

DR. R.C. BILL, TECHNICAL MANAGER

1. Report No.	2. Government Accession No.	3. Recipient's Catalog No.
CR134980		

4. Title and Subtitle	5. Report Date
The Design of Aircraft Brake Systems, Employing Cooling to Increase Brake Life	October 1975
	6. Performing Organization Code

7. Author(s)	8. Performing Organization Report No.
R.P. Scaringe, T.L. Ho and M.B. Peterson	
	10. Work Unit No.

9. Performing Organization Name and Address	11. Contract or Grant No.
Rensselaer Polytechnic Institute Troy, New York 12181	NGR 33-018-152
	13. Type of Report and Period Covered

12. Sponsoring Agency Name and Address	13. Type of Report and Period Covered
	Contractor Report
National Aeronautics and Space Administration Washington, D.C. 20546	14. Sponsoring Agency Code

15. Supplementary Notes

Sponsored by Aerospace Safety Research and Data Institute, Lewis Research Center, Cleveland, Ohio 44135

R.C. Bill, Technical Manager

16. Abstract

A research program was initiated to determine the feasibility of using cooling to increase brake life.

An air cooling scheme was proposed, constructed and tested with various designs. Straight and curved slotting of the friction material was tested.

A water cooling technique, similar to the air cooling procedure, was evaluated on a curved slotted rotor.

Also investigated was the possibility of using a phase-change material within the rotor to absorb heat during braking. Various phase-changing materials were tabulated and a 50%, (by weight) $LiF - BeF_2$ mixture was chosen. It was shown that corrosion was not a problem with this mixture. A preliminary design was evaluated on an actual brake.

Results showed that significant improvements in lowering the surface temperature of the brake occurred when air or water cooling was used in conjunction with curved slotted rotors.

17. Key Words (Suggested by Author(s))	18. Distribution Statement
Friction and Wear Brake Material Brake Design Brake Testing	Unclassified - unlimited

19. Security Classif. (of this report)	20. Security Classif. (of this page)	21. No. of Pages	22. Price*
Unclassified	Unclassified	48	

* For sale by the National Technical Information Service, Springfield, Virginia 22161

FOREWORD

This work was conducted as part of NASA Grant NGR 33-018-152 from the Office of University Affairs, Washington, D.C. 20546. Dr. F.F. Ling, Chairman of RPI's Department of Mechanical Engineering, Aeronautical Engineering & Mechanics was the principal investigator. Acknowledgement is made of the many helpful suggestions made by R.L. Johnson of NASA during the course of this investigation.

The authors were assisted in obtaining experimental data by B.L. Musits of RPI.

TABLE OF CONTENTS

SECTION 1

SUMMARY

A research program was initiated to determine the feasibility of using cooling to increase brake life.

An air cooling scheme was proposed, constructed and tested with various designs. Straight and curved slotting of the friction material was tested.

A water cooling technique, similar to the air cooling procedure, was evaluated on a curved slotted rotor.

Also investigated was the possibility of using a phase-change material within the rotor to absorb heat during braking. Various phase-changing materials were tabulated and a 50%, (by weight) $LiF - BeF_2$ mixture was chosen. It was shown that corrosion was not a problem with this mixture. A preliminary design was evaluated on an actual brake.

Results showed that significant improvements in lowering the surface temperature of the brake occurred when air or water cooling was used in conjunction with curved slotted rotors.

SECTION 2

INTRODUCTION

There are three major areas of concern in present aircraft brake systems, wear, temperature effects and induced friction vibrations.

The brakes are one of the heavier components on an aircraft and there is always an incentive to reduce the size and weight. This tendency has resulted in temperatures approaching the practical limit for the materials in use. Examination of used brakes removed at overhaul shows that the steel rotors have (Rockwell C45 to Rockwell C17) and there is often evidence of plastic distortion. The copper-base brake materials are oxidized throughout which seriously lowers their strength and conductivity. The high temperatures also greatly increase the wear rate. Investigations at RPI show that wear of the current brake material increased rapidly at temperatures above 600°C. There is conclusive evidence that temperatures are higher than this during braking. Clearly, materials are needed that can tolerate higher temperatures and can absorb more energy at a lower temperature.

To solve these problems a high energy brake program has been underway at RPI. Initial studies were concerned with the development of higher temperature, low wear brake friction Materials (Ref.1), improved pad design to make them more compliant (Ref.2), and analysis of the temperatures and contact areas in sliding (Ref.3).

It was proposed to extend this work into the area of innovative braking concepts. That is to design higher temperature braking systems. Consideration was given to new materials, and auxiliary cooling. A test rig was constructed to evaluate a complete brake. See Figure 1 for a schematic diagram of the test equipment and Figure 2 for a photograph of the test equipment. The rig is of such a design that it can be modified appreciably to evaluate new braking concepts and configurations. Several braking concepts were designed and evaluated. These are as follows:

1. Cooling

There is conflicting evidence on the advantages and disadvantages of cooling either in the air, on the ground, or during braking with either gas or water. A review of this experience was made and specific experiments conducted to determine their effectiveness both in cooling and in additional weight

1 – WHEEL HALF
2 – DISC BRAKE
3 – PRESSURE TRANSDUCER
4 – STRAIN GAGE TORQUEMETER
5 – THERMOCOUPLES
6 – TACHOMETER
7 – SOLENOID VALVE
8 – REGULATED COMPRESSED AIR SUPPLY

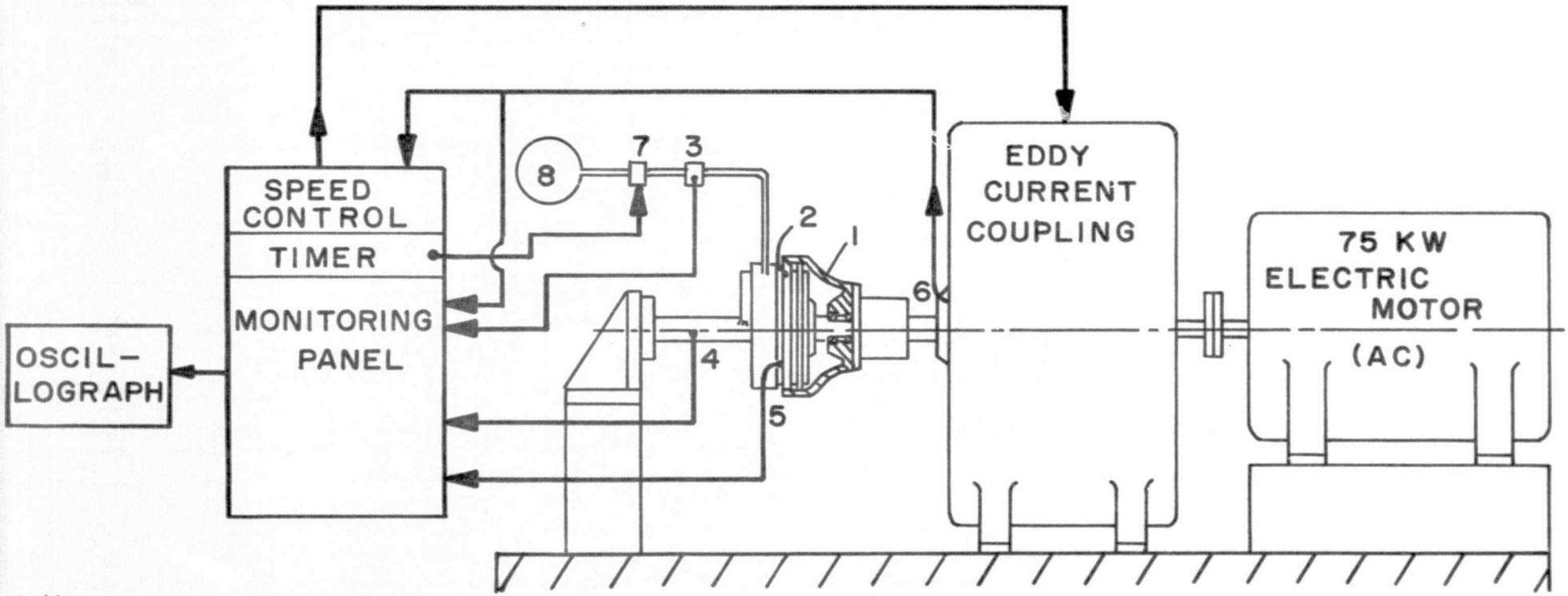

Figure 1 Schematic Diagram of Test Equipment

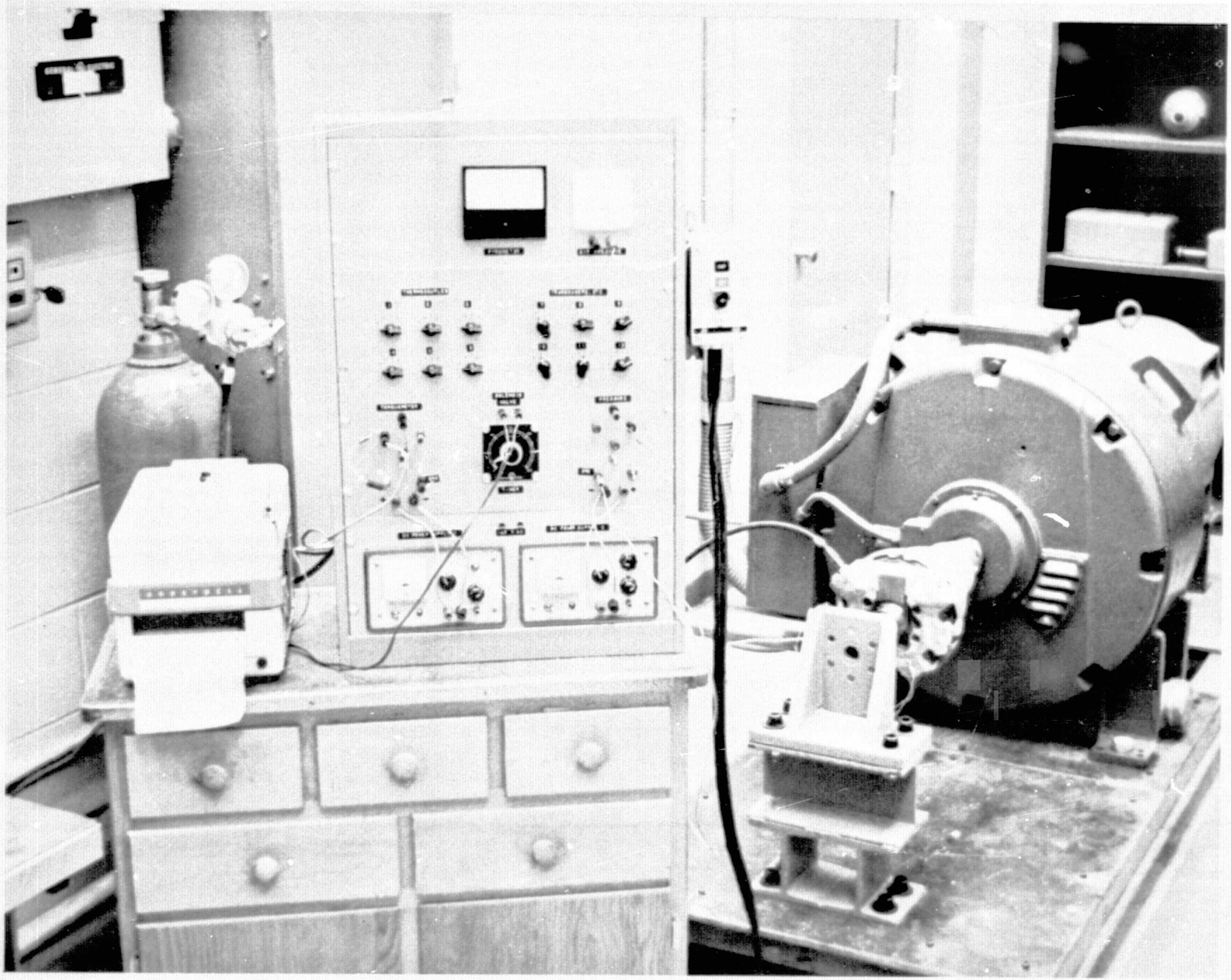

Figure 2 Photograph of the Test Equipment

to be carried. Specifically both an air cooled brake and a water cooled brake were evaluated. Temperatures and friction torque were measured as well as wear. It was necessary to determine the extent to which temperatures can be lowered and how this would affect wear and material requirements in order to assess the effectiveness of the cooling schemes.

2. Fluoride-Filled Rotor System

In this system a fluoride filled rotor replaces the solid rotors currently in use. The rotor was constructed hollow and filled with a material which will absorb considerable energy in a change of state. This, in effect, increases the specific heat of the system. Fewer fluoride-filled rotors of greater thickness were proposed. The loss of braking area with fewer rotors is compensated for by increasing the load by a suitable factor. The higher load gives better surface conformity and more efficient braking. A rotor was constructed and compared with the results of a multiple rotor system using the same materials. First an analysis of such a system was made to determine if the temperatures, wear rates, and braking torque are realistic when using practical construction materials. In particular, it was necessary to observe whether a significant reduction in surface temperature would result.

SECTION 3

APPARATUS, PROCEDURE AND DESIGN

Apparatus

The test rig consists of: an actual brake, (from a small commercial jet plane), a 175 Kw water cooled eddy current speed controller, and a 75 Kw AC electric motor. A photograph of the brake modified to incorporate air and water cooling, is shown in Figs. 3-1 and 3-2. Figure 4 shows a sectional view of this brake system. It is composed of two steel stator plates containing annular friction pads, these two stators sandwich the rotor disk. The rotor is splined outward into the wheel half which is fixed on the shaft of the coupling. The eddy current speed controller allows the rotor to be rotated at any rpm, up to the maximum of 1700 rpm. The dimensions of the rotor and stator are shown in Figures 5 and 6, respectively. Figure 7 indicates the dimensions of the friction pad and fastener. Also shown in Figure 7 is their assembly in the stator plate. This assembly is performed hydraulically on a small hand press, (a load of 2.22×10^4 Newtons is applied to each fastener).

The braking load is applied by compressed air through a solenoid valve actuated by an electronic timer, therefore the braking time is controlled automatically.

Measuring System

A torquemeter, consisting of four strain gages, is mounted on the shaft connecting the two stators to the platform.

A semiconcudtor pressure transducer is located in the air supply line to the brake clamping mechanism.

Angular speed of the rotor is determined from a tachometer mounted in the eddy current coupling.

Approximate surface temperature measurements are obtained from seven chromel - alumel thermocouples installed within 1.59 mm of the sliding surface in four of the 24 friction pads located on the stators. The geometrical location of these thermocouples is shown in Figure 8.

Figure 3-1 Air Cooling System

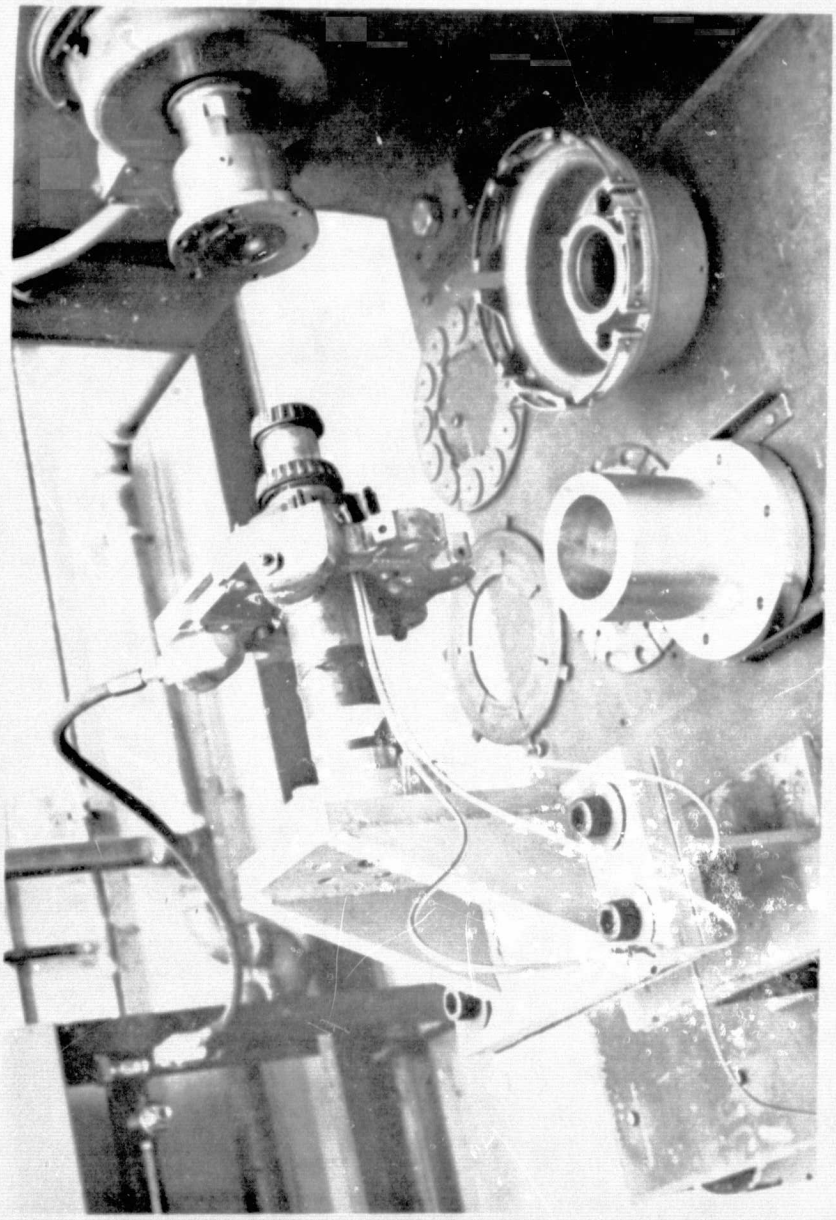

Figure 3-2 Brake with Air Cooling Modifications

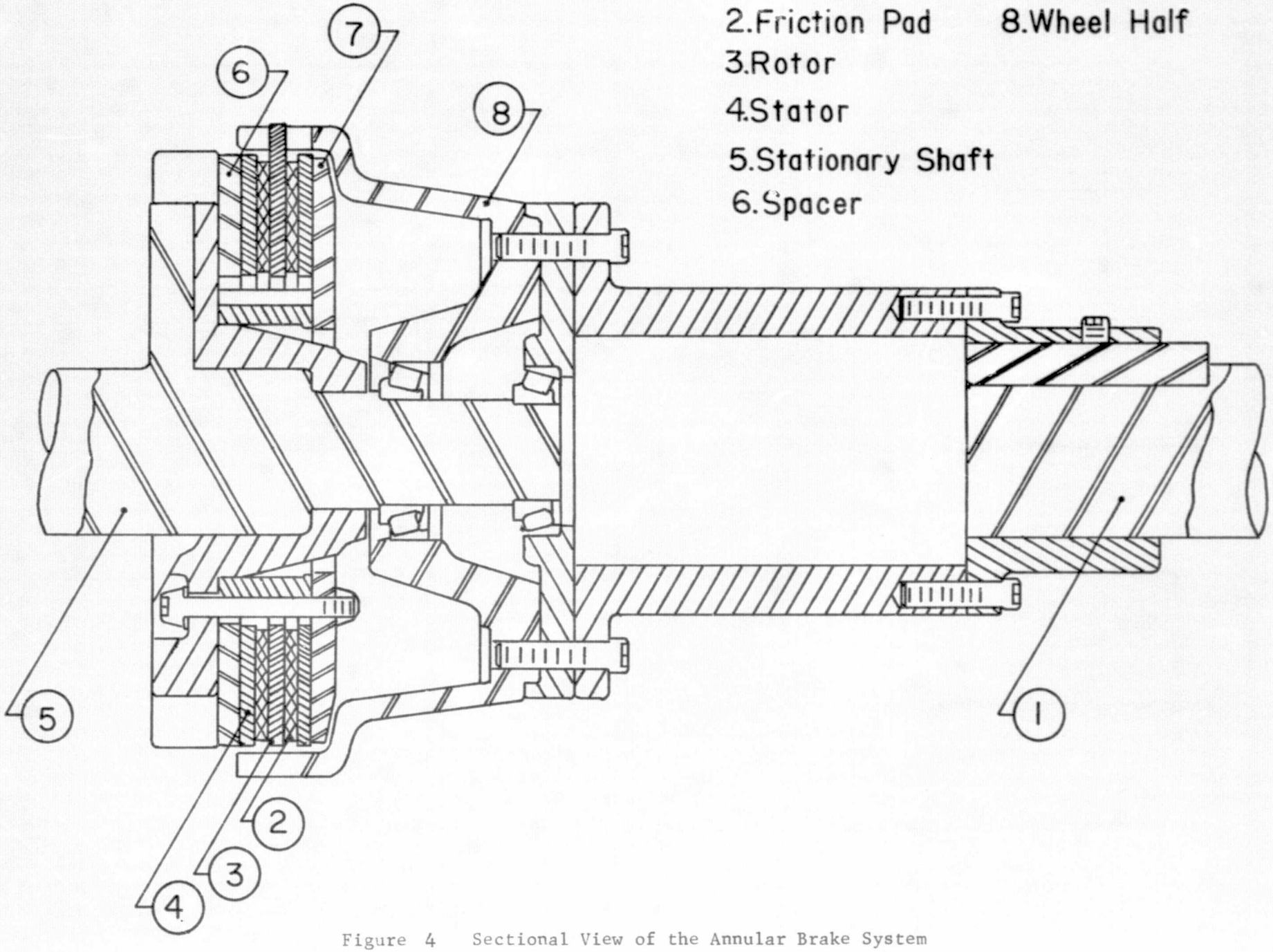

Figure 4 Sectional View of the Annular Brake System

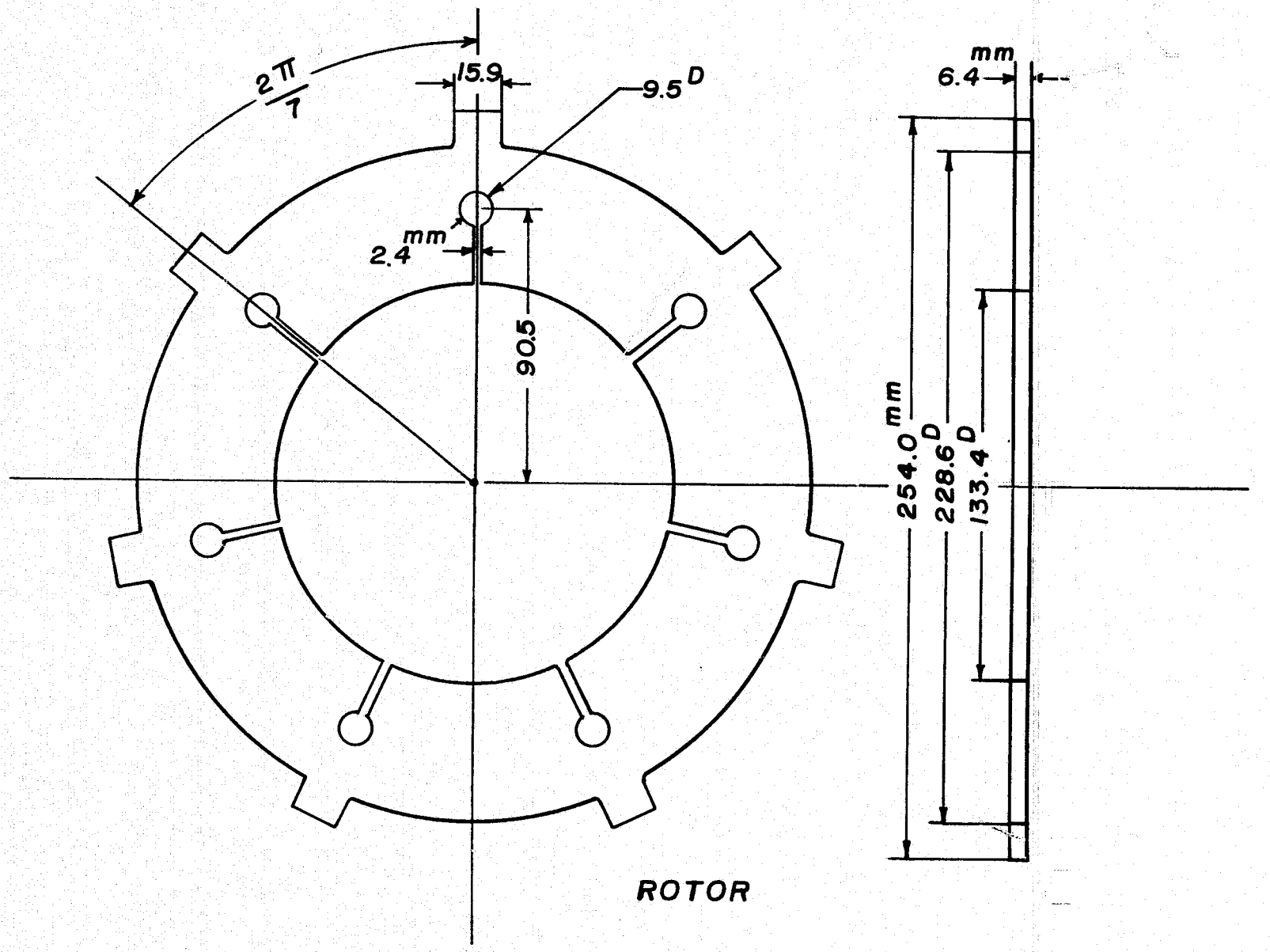

Figure 5 Diagram of Rotor Disk for Button and Pad Brakes

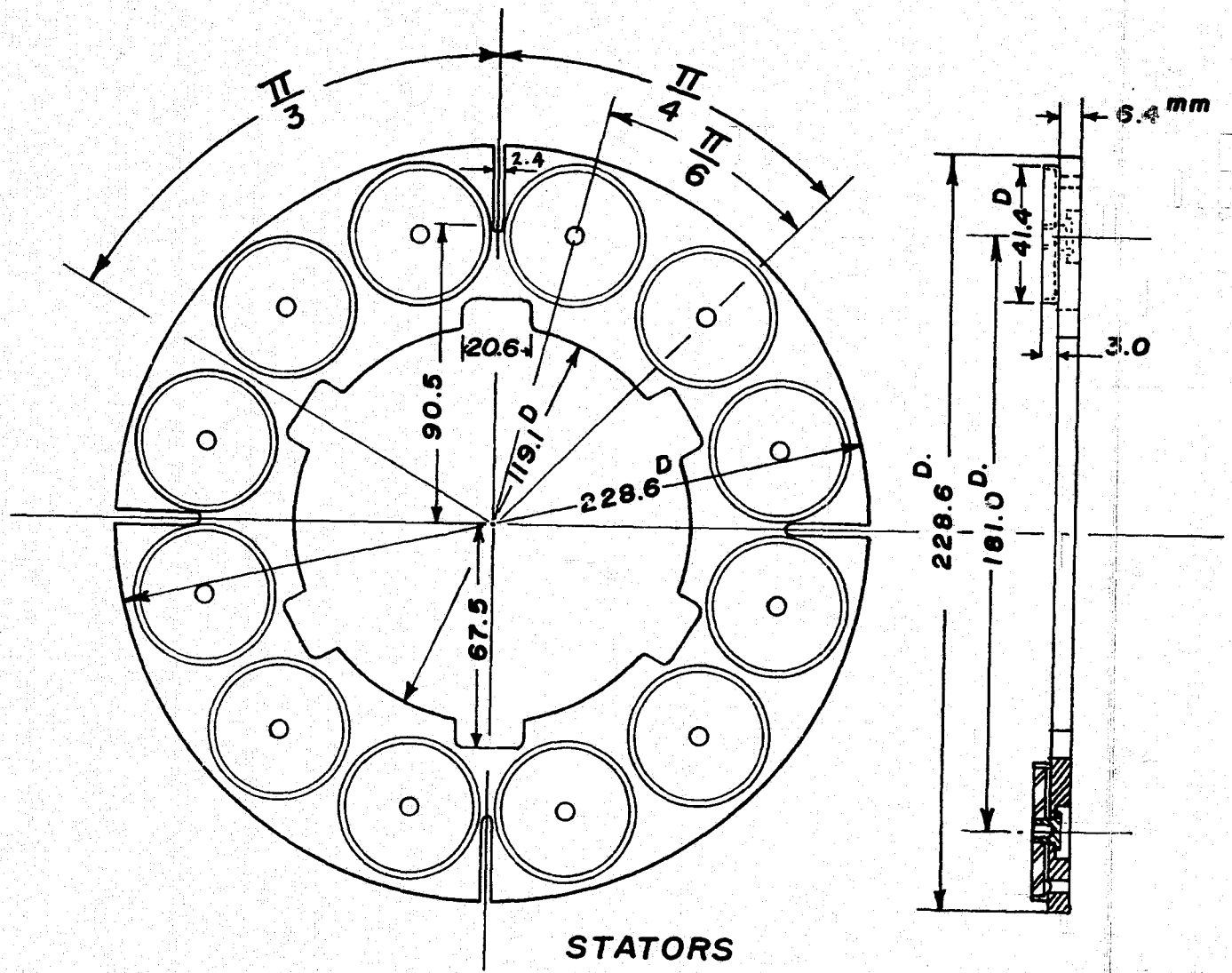

Figure 6 Diagram of Stator for Pad Brake

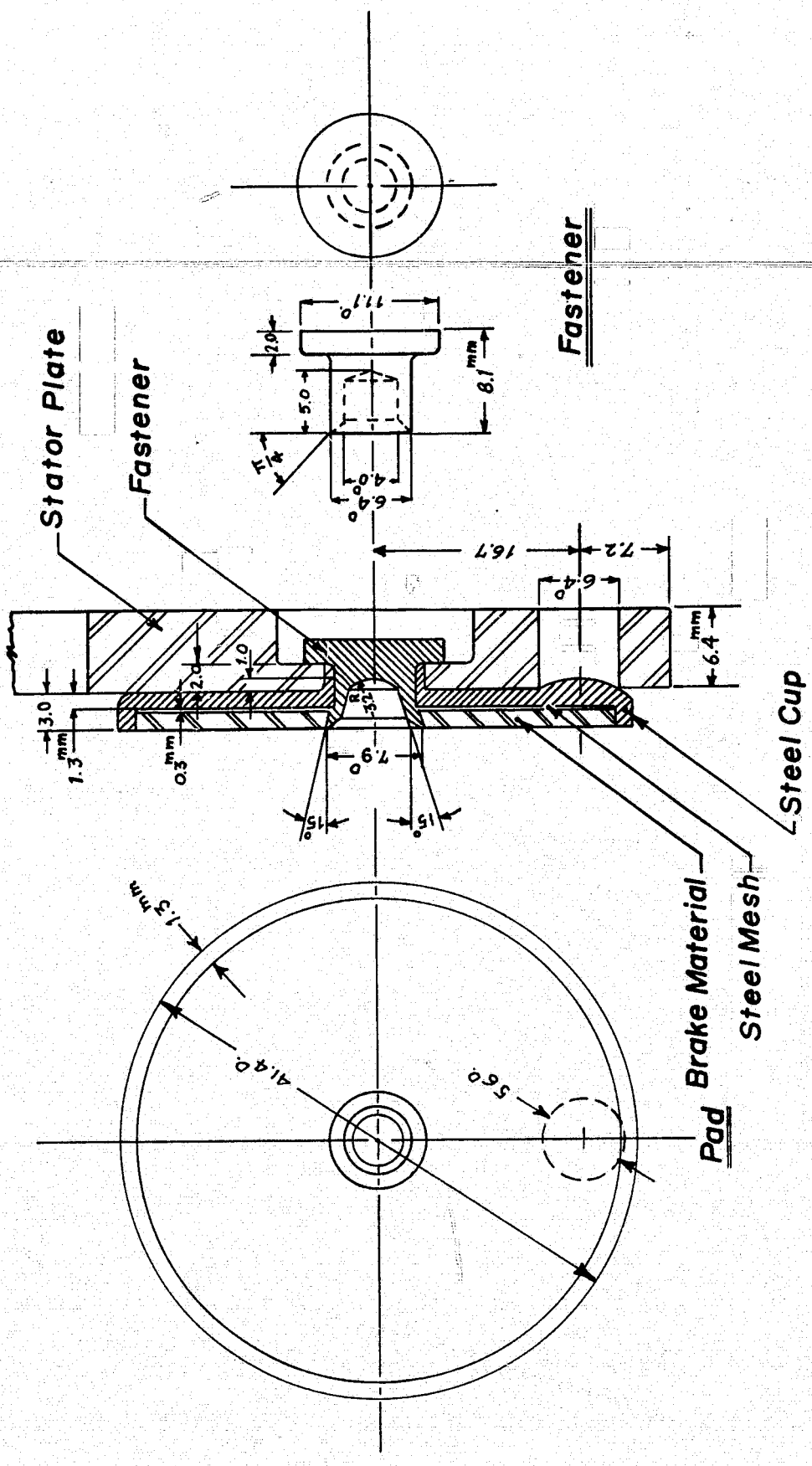

Figure 7 Assembly of Stator Friction Pads

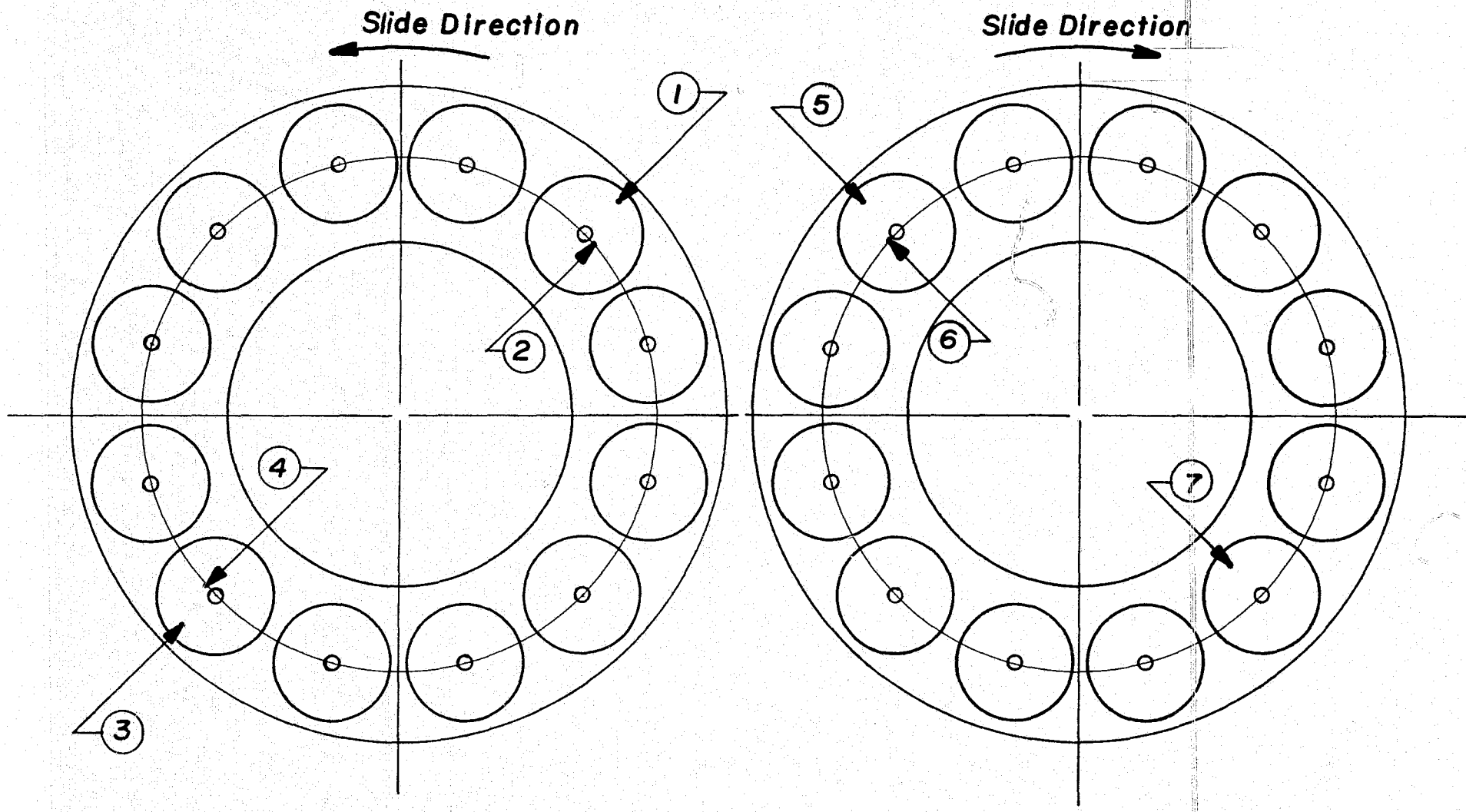

Figure 8 Location of Thermocouples in Pad Brake Stators

The data obtained from these four measuring devices, namely, torque, braking pressure, rpm, and temperature (in seven locations) are continuously recorded simultaneously on a 12-channel oscillograph recorder during the entire braking period.

Procedure and Designs

The rotor disk is surface-finished to approximately 32 rms, and cleaned with solvent. Then it and two stators are weighed and assembled in the brake. The whole rig is always well aligned before running to avoid any vibrational damage. The braking scheme was evaluated under several different braking conditions by varying: applied load (braking pressure), velocity and slide time. The basic test procedure for each braking configuration consisted of the following four series of tests:

1. - Low load (3.24×10^3 N), low speed (850 rpm) for 30 seconds.
2. - Low load (3.24×10^3 N), high speed (1700 rpm) for 30 seconds.
3. - High load (6.31×10^3 N), low speed (850 rpm) for 20 seconds.
4. - High load (6.31×10^3 N), high speed (1700 rpm) for 20 seconds.

For each of the above four series, five tests are performed, (total of 20 tests). The stators and rotor are removed after each series and reweighed to determine wear. The sliding surfaces are inspected for damage.

There are five brake configurations to be tested: air cooling-no slots, air cooling-straight slots, air cooling-curved slots, water cooling-curved slots and fluoride-filled rotors.

Air Cooling

To determine if there exist any benefits in brake life by air cooling, the following scheme was used:

Air was piped into the core of the brake by means of a 2.38 mm (3/32") diameter U-shaped stainless steel tube containing 12 uniformly spaced 0.75 mm (0.0295") diameter holes, (see Figure 9). It is supplied from both ends by a 4.76 mm (3/16") diameter stainless steel tube connected to four 1.38×10^7 N/m^2 (2,000 psi), 6.51 m^3 (230 cubic feet) air cylinders through a regulator and

Figure 9 Stator Support with Air Cooling Manifold

pressure gage. During the test, air pressure was monitored visually by using this gage and maintained at 3.44×10^6 N/m^2 (500 psi). This scheme allows expansion cooling as air leaves the small outlets toward the brake.

The pad brake as previously described was used. The results were compared with the work in Ref.4, for no air cooling, to determine if any significant improvements occur.

Also the same pressurized air cooling tests were run with slotted annular brakes. A brief description of the brakes follows.

Straight Slotted Annular Brake. This brake is a modified design of an annular brake which is conventionally used in the disk brakes of a number of small jet aircraft (see Ref.4). Both brake stators consist of twelve trapezoidal pads fastened to an annular disk (Figure 10). The pads were made of a high temperature alloy of 17-22 AS steel. Seven thermocouples were installed as shown in Figure 10. Similarly, each of the thermocouples was mounted within 0.25 ~ 1.0 mm from the sliding surface. The friction material is annularly bonded to both sides of a steel rotor disk. Twenty-one equally spaced straight slots, each 6.4 mm wide were milled on each face of the rotor, as shown by the dotted lines in Figure 11.

Curved Slotted Annular Brake. This brake is nearly the same as the brake described above. However, the curved slots are used instead of straight ones. The curved slotted rotor (Figure 12) contains 14 curved slots whose area approximates the area of the 21 straight slots. The shape of the curved slots was determined from centrifugal pump theory.

Similarly, the results were compared with those obtained for straight slotted annular brakes without air cooling effects.

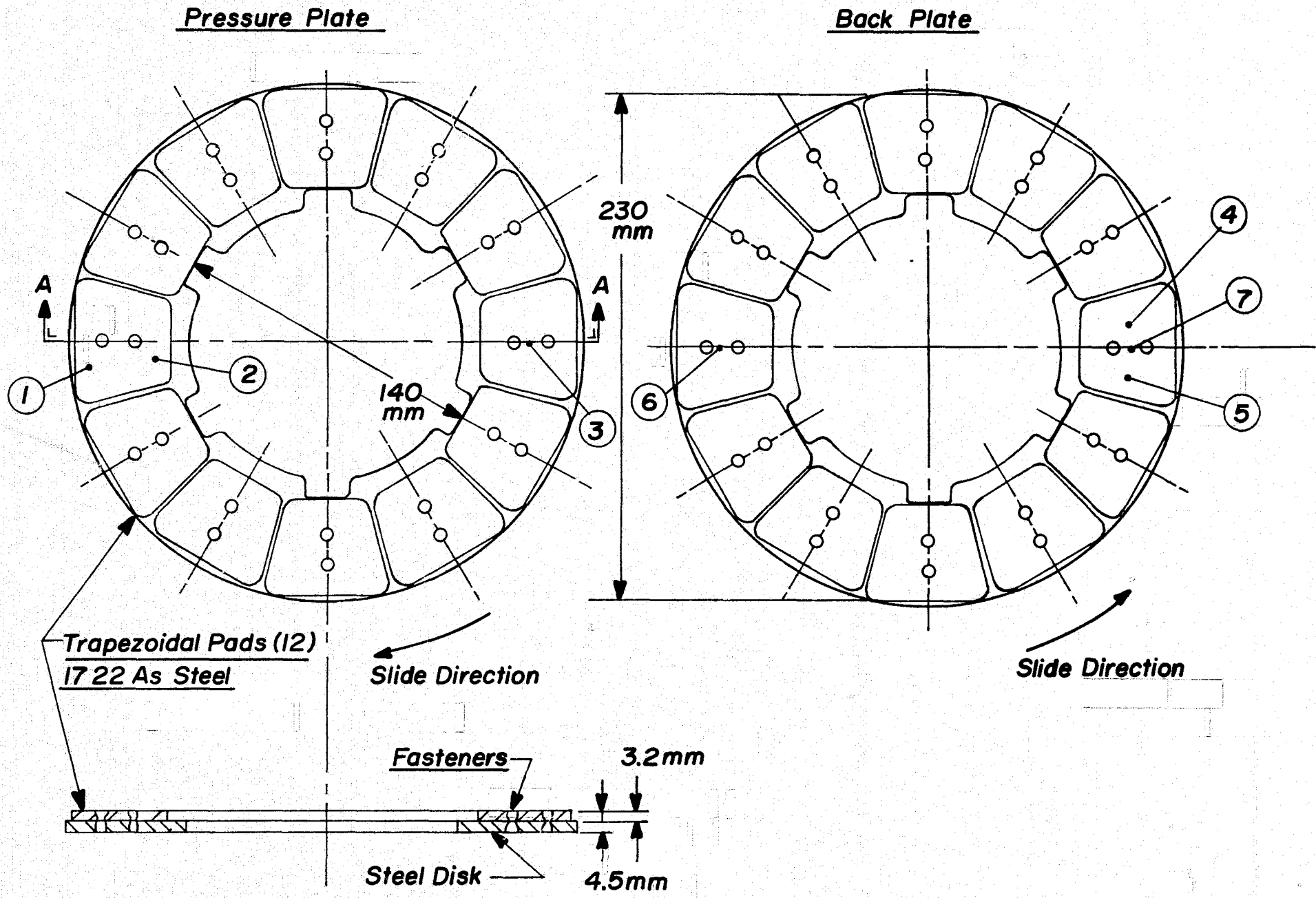

Figure 10 Stator Disks for Annular and Slotted Annular Brakes, Showing Locations of Thermocouples

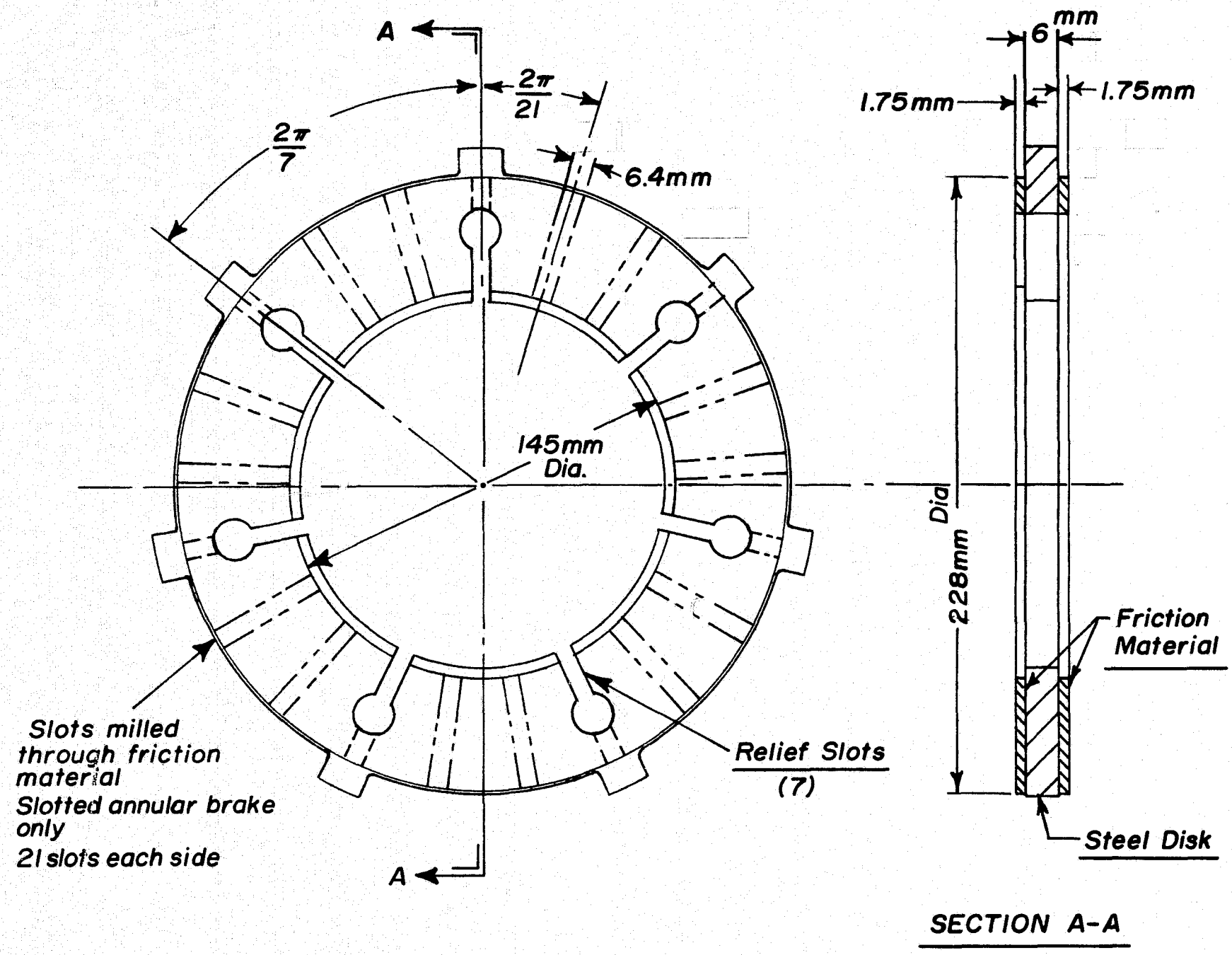

Figure 11 Rotor Disk Used in Annular and Slotted Annular Brakes

A 51° 25' 43"
B 48°
C 33°
D 4.13 cm.

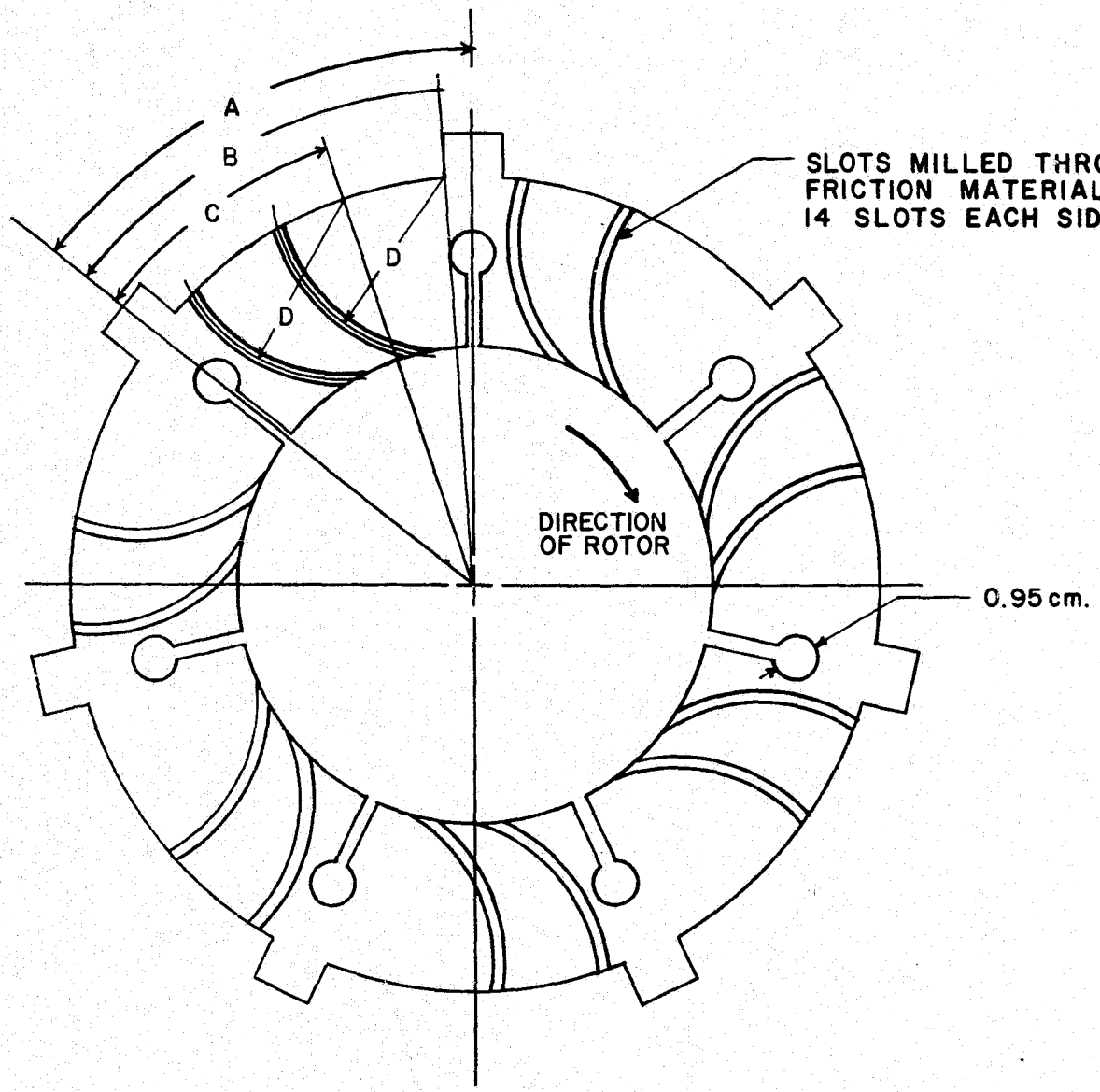

Figure 12 Curved Slotted Rotor

Water Cooling

Water was supplied to the core of the brake by means of the same supply line as used for air. This time, however, it was supplied (from both ends) by a 4.76 mm (3/16") diameter stainless steel tube connected to a 4.55×10^{-3} m^3 (1 gallon) water tank and pressurized to 1.38×10^6 N/m^2 (200 psi). This pressure is maintained constant throughout the test by a regulator and air cylinder.

The water cooling was used only for the curved slotted annular brake described above.

Fluoride Filled Rotor System

An analysis of present compounds was performed to obtain a substance with a melting point below 600°C, and a high density and heat of fusion combination. Previous work in RPI's Tribology Laboratory (Ref.5) has shown that due to poor external dissipation of heat from the brake, the specific heat and the density are the most important factors. Since we are considering a material which will undergo a phase change, the heat of fusion is analogous to the specific heat during the phase change.

The two important parameters used for such an evaluation are therefore ρC and ρH_f (ρ = density, C = specific heat and H_f = heat of fusion). Values of these were collected for a large number of substances. The more promising substances are listed in Table I (Refs.6,7,8 and 9).

It is evident, from Table I, that compounds and binary alloys are superior to pure metals from a heat absorbing standpoint. It can also be seen that the eutectic mixture of 50% (by weight) LiF and BeF_2 is the most promising.

This combination can absorb 61% more heat, in a temperature rise from 21°C to 660°C than an equal sized Beryllium brake.

It must be determined how long it will take for the entire core of the brake rotor to melt. This was done by deriving an expression for the rate of solid and liquid boundary movements (see Appendix II).

For the purpose of testing and evaluating the capabilities of the hollow rotor system, the following test design was proposed: A 1.91 cm (3/4") thick 17-22 AS steel rotor containing 21 pockets was filled with the LiF-BeF_2 mixture. The design is shown in Figure 13 and the actual rotor is shown in Figure 14. Before construction of an actual rotor a test sample of 17-22 AS steel filled with LiF-BeF_2 was thermally cycled from 30°C to 700°C and it was determined that corrosion was not a problem.

TABLE I

POSSIBLE HEAT STORAGE MIXTURES

Substance	Melting Point (°C)	Density (gm/cc)	Density × Heat of Fusion (cal/cc) [1]	Density × Heat Capacity (cal/cc°K) [1]	Total Heat Absorbed During 21°C to 660°C Temp. Rise (cal/cc)
Compounds					
50% LiF 50% BeF_2 (by wt.)	360.	2.3	352.	.743	827.
LiOH	462.	1.46	151.	.774	645.
KCl - $MgCl_2$	487.	2.14	160.	.762	647.
LiBr	552.	3.46	116.	.495	431.
LiCl	614.	.207	156.	.592	534.
$MnCl_2$	650.	2.98	174.	.450	462.
$NaNO_3$	310.	2.26	100.	.565	460.
Binary Alloys [2]					
Al - Cu 67% Al	548.	4.77	233.	.711	687.
Al - Zn 95% Zn	382.	6.92	177.	.69	618.
Ca - Cu 63% Cu	560.	6.34	176.	.70	623.
Cu - Mg 65.4%	552.	6.46	213.	.78	711.
Metals					
Zn	419.5	7.0	189.	.651	415.
Be [3]	1285.	1.85	599.	.807	515.

Notes

1) For an explanation of heat capacity and heat of fusion calculations, for alloys, see Appendix I.

2) Phase separation may be a problem with the binary alloys. If so, some of the constituents may not melt until very high temperatures.

3) Beryllium is included here to indicate the relative orders of magnitude of the substances in the table. Its melting point is too high to be considered as a possible phase change material.

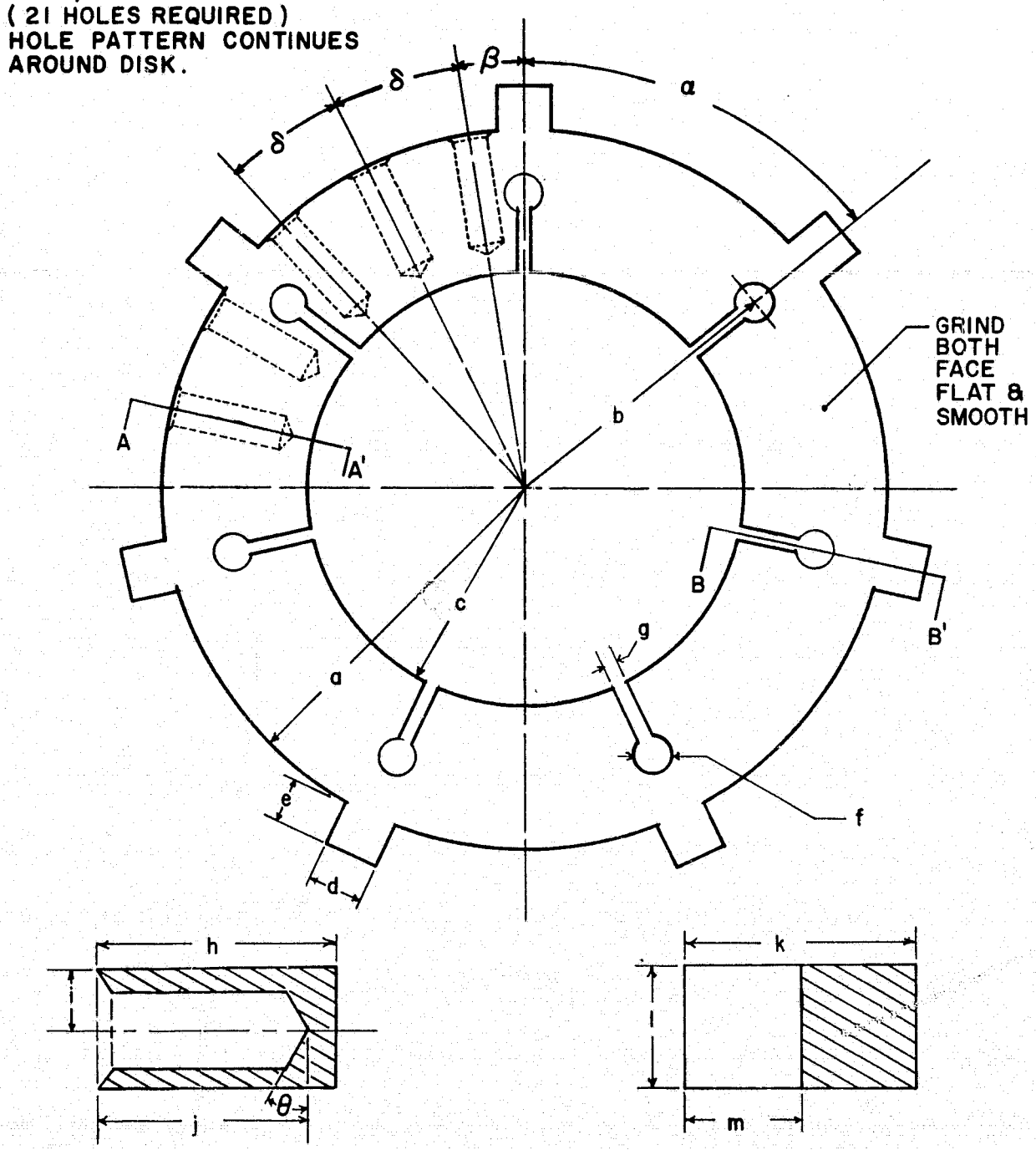

Section A-A'

Section B-B'

a - 11.43 cm	f - 0.64	k - 6.03	δ - 16°41'
b - 8.89 cm	g - 0.32	l - 1.91	θ - 30°
c - 6.35	h - 4.76 ± 0.04	m - 2.54	
d - 1.59	i - 0.95	α - 51°25'	
e - 1.27	j - 4.45 ± 0.15	β - 9°	

Figure 13 Hollow Rotor

Top View

Front View

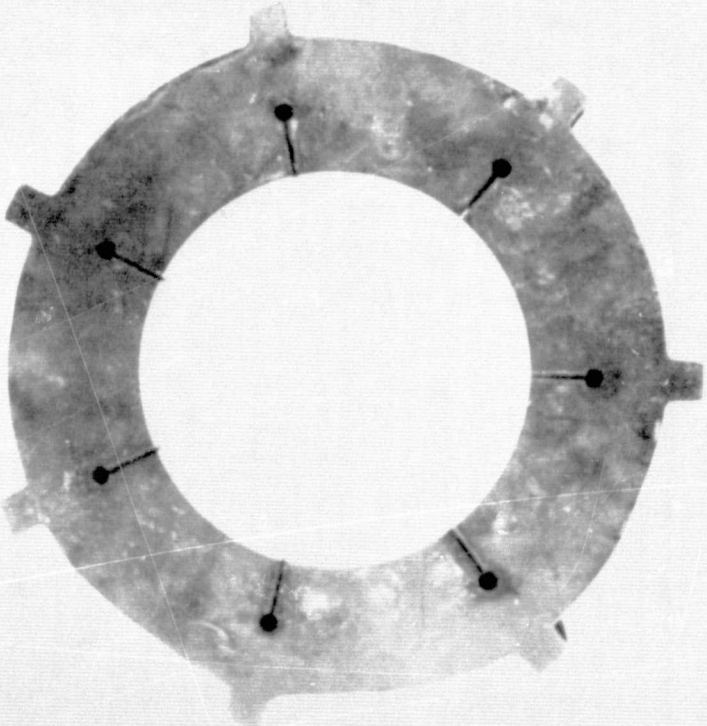

Figure 14 A Photograph of the Actual Rotor

SECTION 4

RESULTS AND DISCUSSION

Three sets of tests were run in order to evaluate the application of an air or water cooling, the design of slotted rotors, as well as the concept of the filled rotor. All the results were obtained for the copper based brake material rubbed against 17-22 AS steel. They are presented and discussed in the following sections.

Air Cooling

As mentioned in the last section, the pad brake and slotted annular brakes were applied during the evaluation phase of this work. Therefore two separate sets of comparisons were made as follows:

(1) Pad Brake Tests. The pad brake was used to find the cooling effect of pressurized air. Here expansion cooling of this compressed air was expected. The test results were tabulated in Table II. They were also compared with those of previous work (Ref.4), in which the same pad brakes were used but no air cooling applied. Comparison of these data are shown in Figures 15 and 16.

As shown in Figure 15, no cooling effect is indicated. It is felt that the contact of both mating surfaces was so intimate that there was no path for the air to pass and carry the frictional heat from the interface. Therefore, the design of slots on both surfaces of the rotor disk was necessary. This will be discussed later. No notable change of wear or friction due to the cooling was found (see Fig.16)

(2) Slotted Annular Brake Tests. The compressed air cooling scheme was maintained the same in these tests. First, the straight slotted friction material rotor was used, sliding against steel pads. The summary of results is listed in Table III. Also they are compared with those of the work in Ref.4, which were obtained for the same brake but under the condition of no air cooling (see Figs.17 and 18). The curve for no air cooling is designated "1" and that with air cooling is designated "2" in the figures. In Figure 17, the temperature points of curve "2" show even higher than those of "1". This means that the design of straight slots on the rotor did not assist air in passing through to absorb frictional heat from the contact zone. The reduction

TABLE II

EVALUATION TEST SERIES FOR A COPPER BASE FRICTION MATERIAL WITH PRESSURIZED AIR COOLING

Test Series # *		1	2	3	4
Apparent Pressure of Contact (N/m^2)		2.17×10^5	2.17×10^5	4.12×10^5	4.02×10^5
Angular Velocity (rpm)		808.	1640.	813.	1640.
Slide Time (seconds)		30.	30.	20.	20.
Final Coefficient of Friction		.499	.358	.428	.256
Average Surface Temperature (°C)		387.	554.	429.	572.
Frictional K.E. (joules)		7.55×10^5	11.52×10^5	7.81×10^5	11.47×10^5
PV (N/m^2) • (rad/sec)		1.84×10^7	3.73×10^7	3.51×10^7	6.91×10^7
Stator	Total Wear (grams)	.78	4.184	1.072	6.606
	Wear Rate (gm/sec)	.0529	.1395	.0536	.3303
Rotor	Total Wear (grams)	.062	2.288	.312	2.700
	Wear Rate (gm/sec)	.0021	.0763	.0156	.1350

* Average values from five tests.

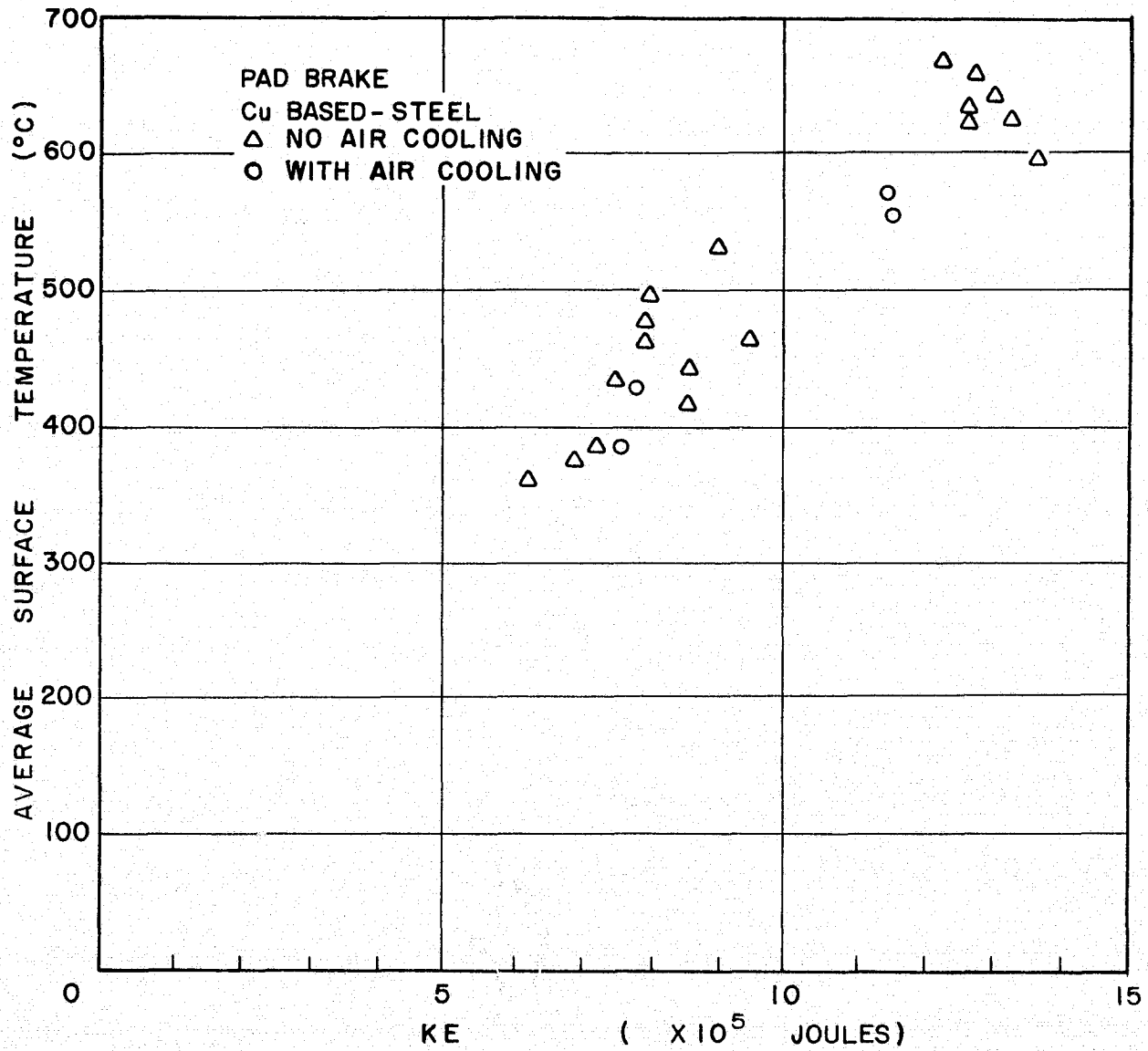

Figure 15 The Effect of Total Frictional Kinetic Energy on the Surface Temperature of the Friction Materials

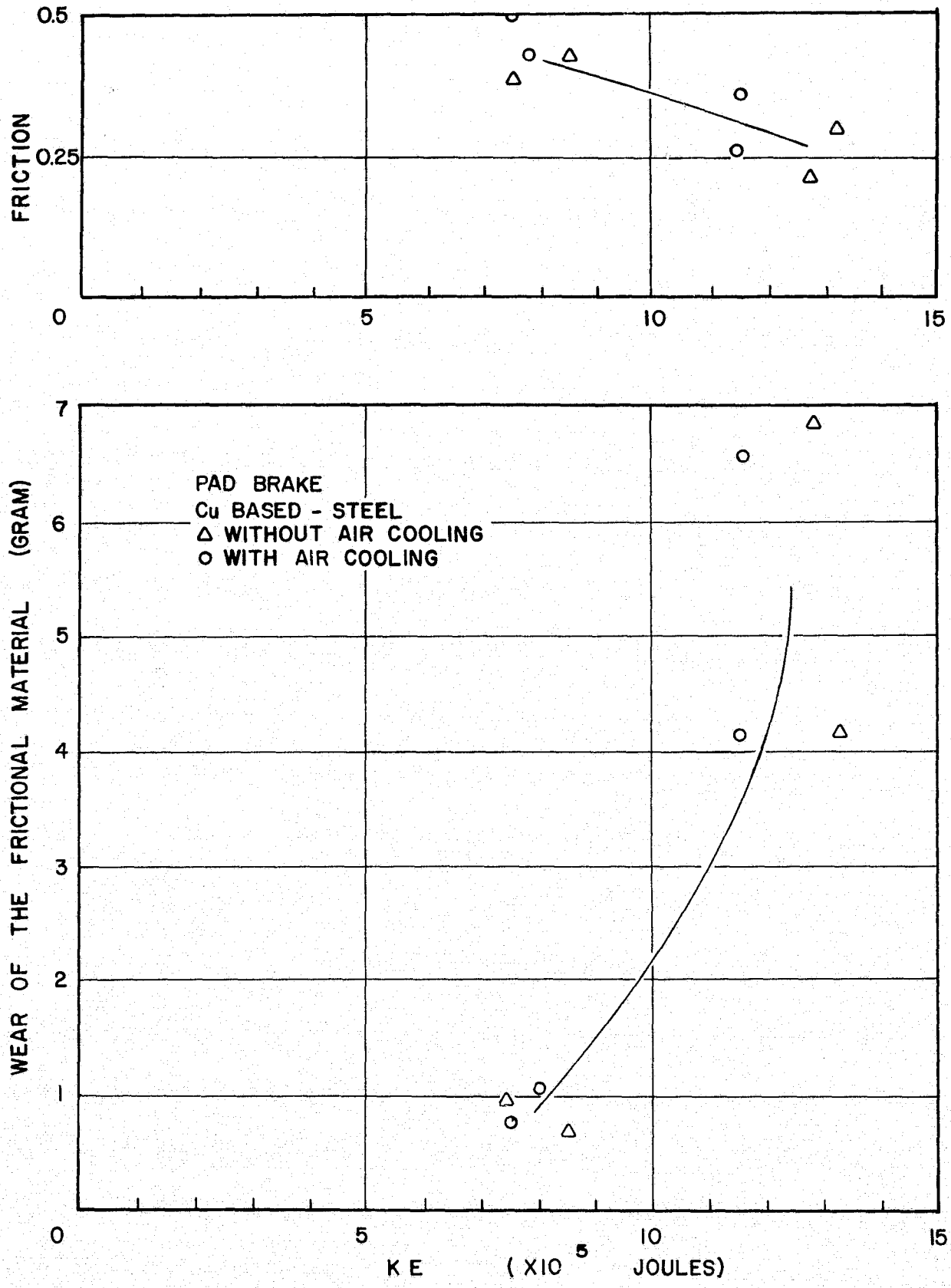

Figure 16 The Effect of Total Frictional Kinetic Energy on Wear and Friction of the Friction Materials

TABLE III

EVALUATION TEST SERIES FOR A COPPER-BASE FRICTION MATERIAL EMPLOYING PRESSURIZED AIR COOLING AND A STRAIGHT SLOTTED ROTOR

Test Series		1	2	3
Apparent Pressure of Contact (N/m^2)		2.2×10^5	2.2×10^5	4.3×10^5
Angular Velocity (rpm)		850	1700	820
Slide Time (Seconds)		30	30	20
Final Coefficient of Friction		.32	.30	.29
Average Final Surface Temperature (°C)		322	477	379
Frictional Kinetic Energy (Joules)		5.06×10^5	8.8×10^5	5.62×10^5
PV (N/m^2) • (rad/sec)		1.97×10^7	3.94×10^7	3.64×10^7
Frictional Material	Total Wear/Run (gr)	.63	1.59	.75
	Wear Rate/ Run (gr/sec)	.021	.053	.038
Steel 17-22 AS	Total Wear (gr)	.70	.39	1.09
	Wear Rate (gr/sec)	.023	.013	.055

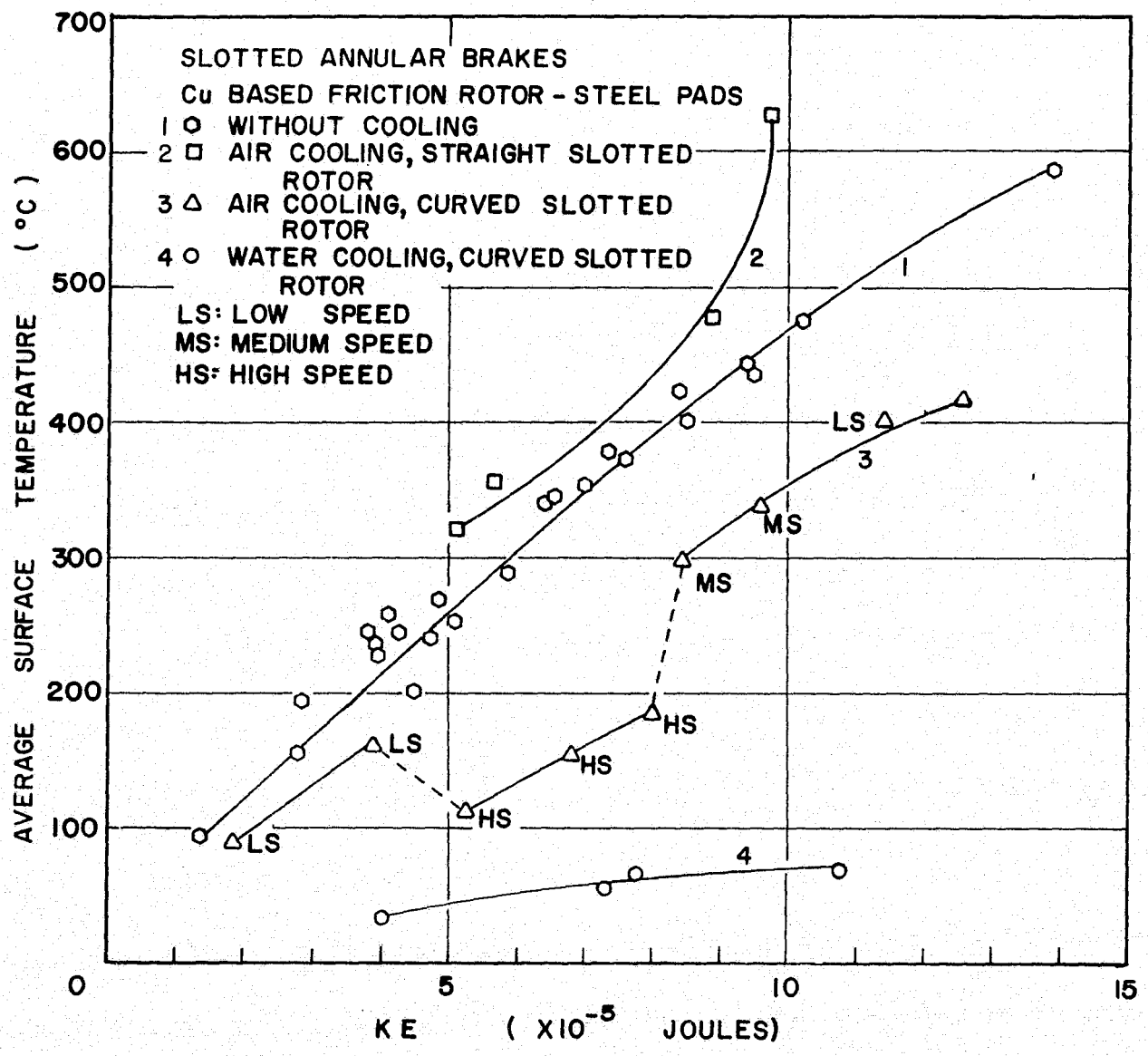

Figure 17 The Effect of Total Frictional Kinetic Energy on the Surface Temperature of the Friction Materials

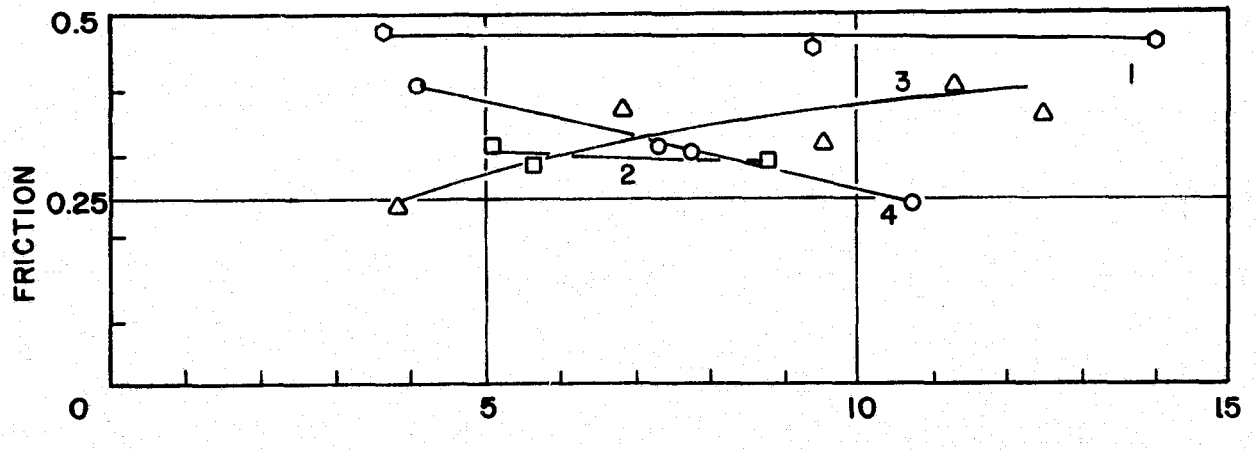

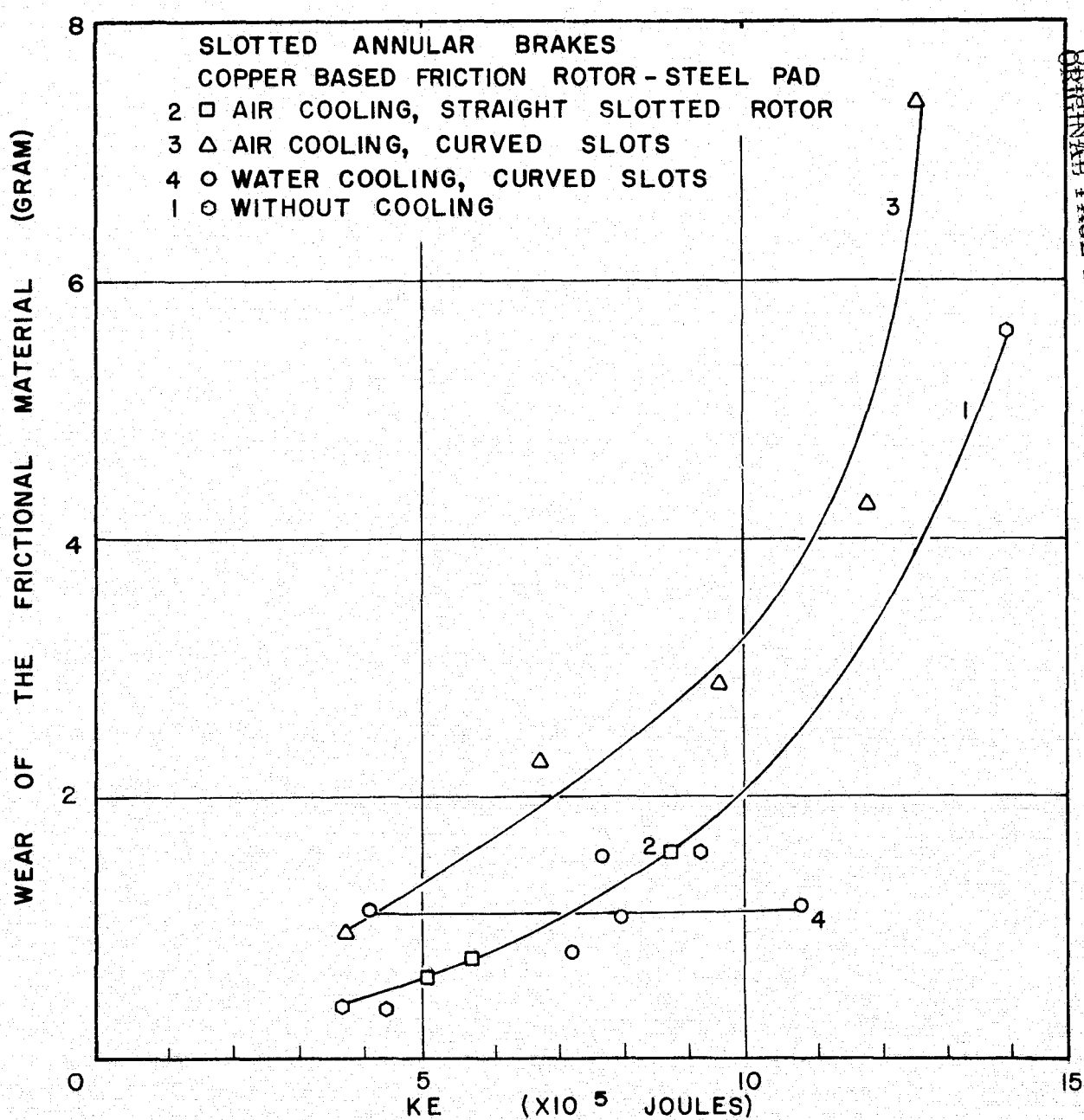

Figure 18 The Effect of Total Frictional Kinetic Energy and Wear and Friction of the Friction Materials

of contact area because of slotted design resulted in slightly higher temperatures. No change of wear was found (Fig.18).

In order to have air pumping, the design of curved slots in friction rotor was employed and evaluated. The results are summarized in Table IV. Similarly, they are plotted and designated as curve 3 in both Figures 17 and 18. The cooling benefit is indicated in Figure 17 with application of this curved slotted design. Also it is seen that lower temperatures were obtained for maximum operative speed at 1750 rpm. These points deviate from the other sections of curve "3", which were obtained for tests at medium speed (1300 rpm) or low speed (850 rpm). This means that the higher velocity of rotor activation improved pumping of the curved slots.

The slightly high wear was found (Fig.18). This could be the result that a lot of loosening particles were blown away from the interface. Further work is needed for confirmation. An increasing friction curve (3) is shown in the last figure along the basis of energy.

Water Cooling

Only the curved slotted rotor was applied in this water cooling scheme. Therefore, the curved slotted annular brake was used for this phase of the evaluation testing. As mentioned before, 4.55×10^{-3} m^3 (1 gallon) water was supplied during 20 sec braking for each test. The results were tabulated in Table V. The significant data are presented and compared with those of previous works in Figures 17 and 18, (designated curve "4" in each). As expected, the lowest temperature curve is found with water cooling. The average surface temperatures remained below 100°C along the whole frictional energy range, even above the value generated during normal stops (10^6 Joules). The low wear (see Fig.18) is the result of the low temperatures generated. The friction drops linearly from 0.4 to 0.24 with the increasing of the frictional kinetic energy from 4.0 to 10.7×10^5 Joules (Fig.18). At the present time no precise explanation can be given for this effect.

Filled Rotor Concept

A high heat absorbing fluoride substance was selected. Testing of this LiF-BeF_2 eutectic mixture in intimate contact with the 17-22 AS steel, after repeated thermal cycling indicated that corrosion was not a problem.

TABLE IV

EVALUATION TEST SERIES FOR A COPPER-BASE FRICTION MATERIAL EMPLOYING PRESSURIZED AIR COOLING AND A CURVED SLOTTED ROTOR

Test Series		1	2	3	4	5
Apparent Pressure of Contact (N/m^2)		2.1×10^5	4.3×10^5	2.1×10^5	4.2×10^5	4.2×10^5
Angular Velocity (rpm)		840	840	1700	1400	1700
Slide Time (Seconds)		30	30	20	20	20
Final Coefficient of Friction		.24	.40	.37	.32	.36
Average Surface Temperature (°C)		162	403	156	337	417
Frictional Kinetic Energy (Joules)		3.83×10^5	11.3×10^5	6.83×10^5	9.56×10^5	12.51×10^5
PV (N/m^2) • (rad/sec)		1.87×10^7	3.77×10^7	3.79×10^7	5.98×10^7	7.25×10^7
Frictional Material	Total Wear/Run (gr)	.98	4.31	2.30	1.90	7.40
	Wear Rate/Run (gr/sec)	.033	.144	.115	.095	.37
Steel 17-22 AS	Total Wear (gr)	.13	≈ 0	≈ 0	≈ 0	.37
	Wear Rate (gr/sec)	.0043	≈ 0	≈ 0	≈ 0	.0185

TABLE V

EVALUATION TEST SERIES FOR A COPPER-BASE FRICTION MATERIAL EMPLOYING WATER COOLING AND A CURVED ROTOR

Test Series		1	2	3	4
Apparent Pressure of Contact (N/m^2)		2.2×10^5	4.2×10^5	4.3×10^5	2.3×10^5
Angular Velocity (rpm)		800	1700	1000	1700
Slide Time (Seconds)		20	20	20	20
Final Coefficient of Friction		.40	.24	.31	.32
Average Surface Temperature (°C)		34	71	67	56
Frictional Kinetic Energy (Joules)		4.08×10^5	10.74×10^5	7.78×10^5	7.32×10^5
PV (N/m^2) • (rad/sec)		1.86×10^7	7.38×10^7	4.3×10^7	4.0×10^7
Frictional Material	Total Wear/ Run (gr)	1.26	1.26	1.62	.70
	Wear Rate/ Run (gr/sec)	.063	.063	.081	.035
Steel 17-22 AS	Total Wear (gr)	NA	1.18	1.06	.46
	Wear Rate (gr/sec)	NA	.059	.053	.023

A fluoride filled rotor was made (as shown in Fig.14) and evaluated by sliding against two stators with annular round pads of the current copper based friction material. The results are listed in Table VI and compared with those of pad brake tests where a common solid steel rotor was used. No benefit was found from the temperature data (Fig.19) or the friction and wear data (Fig.20). It should be noted that the melting of the eutectic salt appears to correspond with a temporary drop in temperature from 400°C to 325°C during a kinetic energy increase from 6.3×10^5 Joules to 7.7×10^5 Joules. Thermal conductivity of the eutectic salt (Appendix II), or of 17-22 AS steel was not a problem.

The eutectic mixture did not further lower the temperature because it had all melted. The molten salt has a low heat capacity. More fluoride would have to be incorporated into the design of the rotor to further reduce the temperature.

TABLE VI

EVALUATION TEST SERIES FOR A COPPER-BASE FRICTION MATERIAL WITH A LiF-BeF_2 FILLED ROTOR

Test Series		1	2	3	4	5
Apparent Pressure of Contact (N/m^2)		2.1×10^5	2.1×10^5	4.2×10^5	4.2×10^5	4.2×10^5
Angular Velocity (rpm)		850	1700	840	1700	1400
Slide Time (Seconds)		30	30	20	20	20
Final Coefficient of Friction		.46	.20	.32	.30	.39
Average Surface Temperature (°C)		327	394	369	568	541
Frictional Kinetic Energy (Joules)		7.72×10^5	6.34×10^5	7.06×10^5	13.0×10^5	12.7×10^5
PV(N/m^2) • (rad/sec)		1.91×10^7	3.80×10^7	3.70×10^7	7.18×10^7	6.00×10^7
Frictional Material	Total Wear/Run (gr)	1.35	.92	1.18	5.76	2.50
	Wear Rate/Run (gr/sec)	.045	.031	.059	.288	.125
Steel 17-22 AS	Total Wear (gr)	.37	.68	.28	4.58	2.14
	Wear Rate (gr/sec)	.012	.023	.014	.229	.107

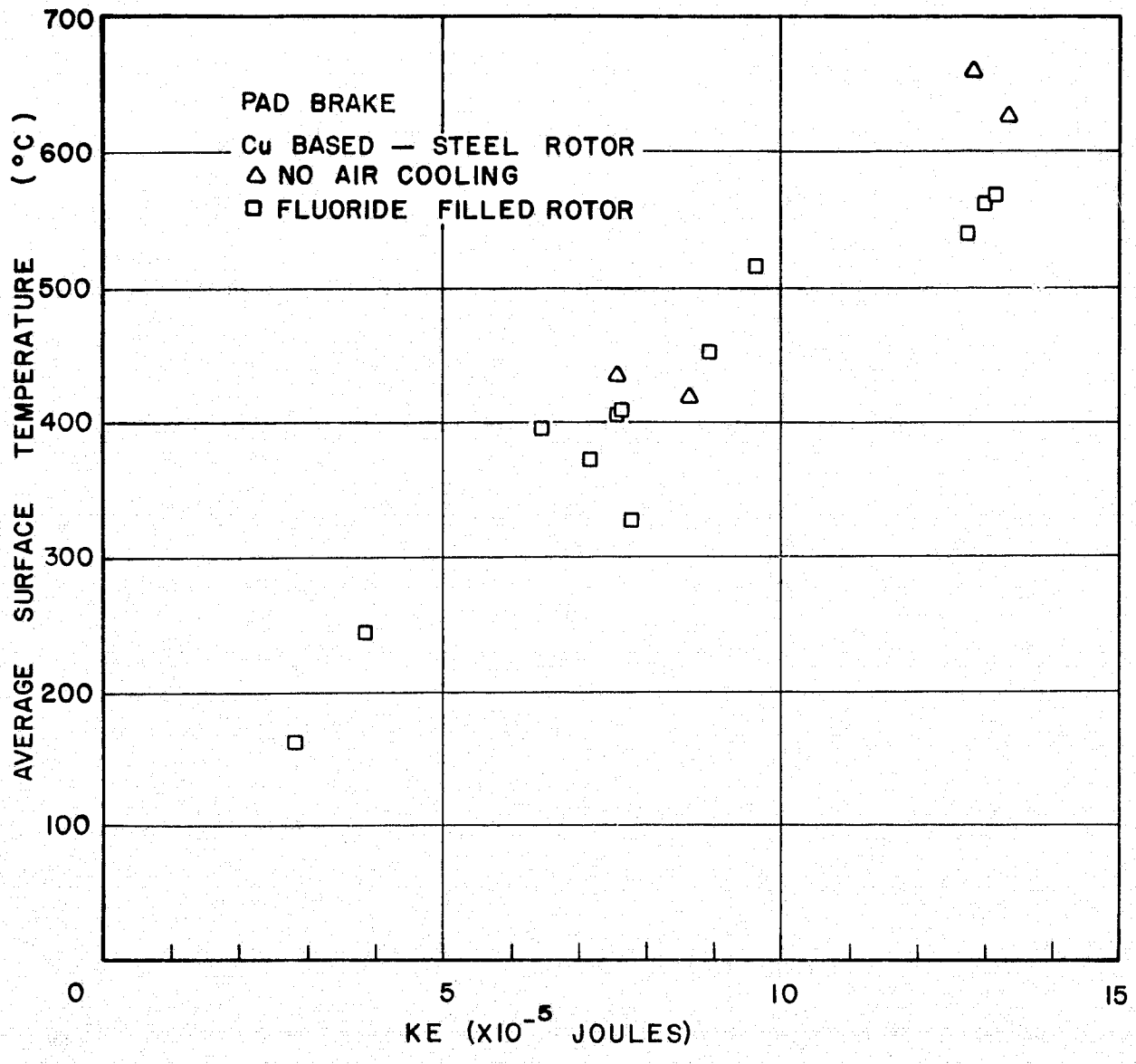

Figure 19 The Effect of Total Frictional Kinetic Energy on the Surface Temperature of the Friction Materials

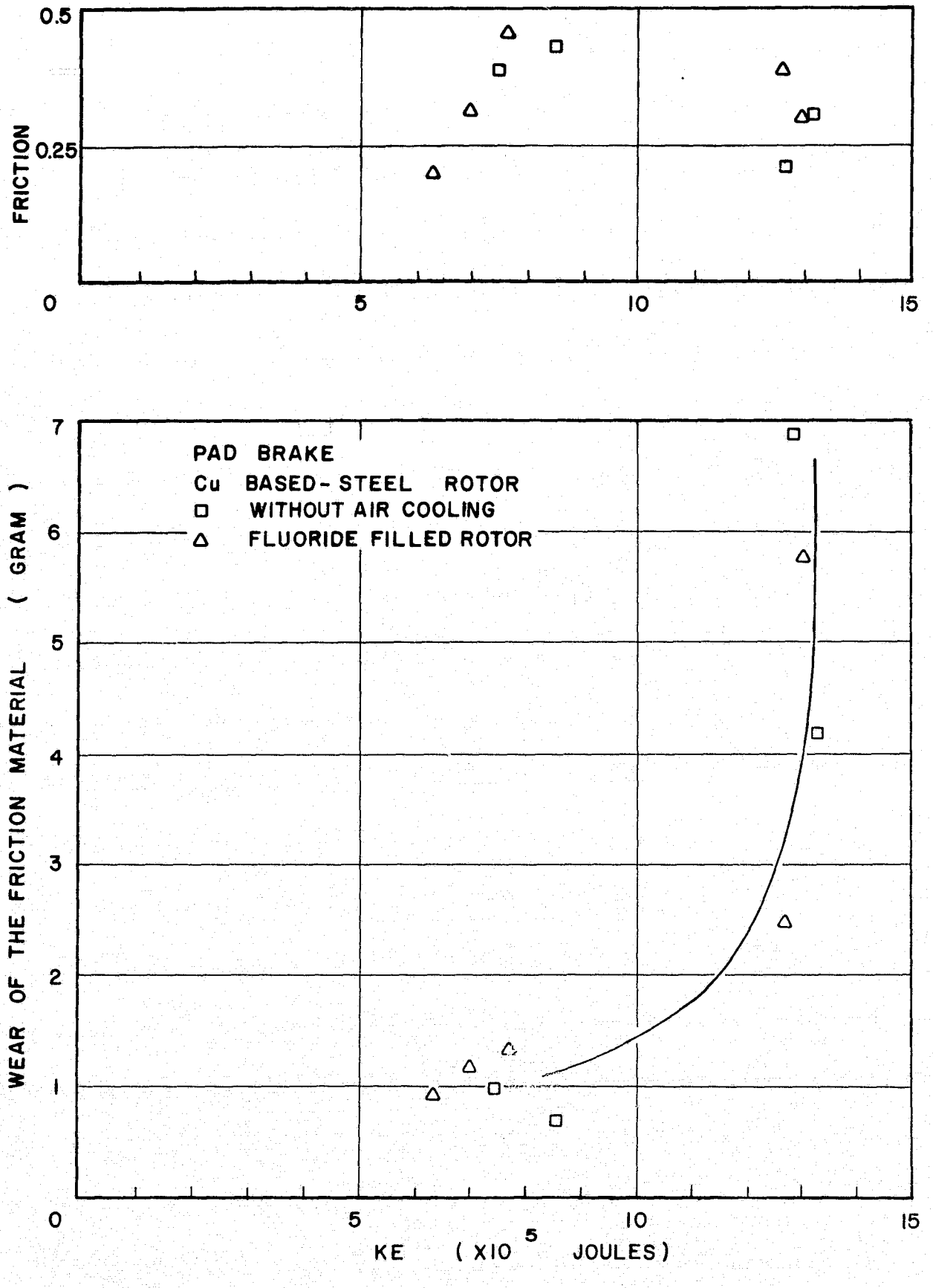

Figure 20 The Effect of Total Frictional Kinetic Energy on Friction and Wear of the Friction Materials

SECTION 5

SUMMARY OF RESULTS

A program has been underway to evaluate several design modifications with the application of air or water cooling or the concept of the filled rotor for use in aircraft brakes. The following results have been obtained for the current copper based materials sliding against 17-22 AS steel:

(1) The pressurized air cooling applied for the ordinary pad brakes yields no improvements in lowering the surface temperatures and wear.

(2) The pressurized air cooling applied for the straight slotted annular brake yields higher temperatures. No cooling benefit is indicated with the application of straight slots on the rotor. The reduction of contact area due to this design results in slightly higher temperatures.

(3) The pressurized air cooling applied for the curved slotted annular brake yields lower temperatures. Air pumping is obtained using curved slots on the rotor; however higher wear is found.

(4) The water cooling applied for the curved slotted annular brake yields the most promise. Using less than a gallon of water, temperature can be reduced by 88% and wear of the friction material can be reduced by 76%. The friction is 0.3.

(5) Based upon an analysis of present compounds, a high heat absorbing fluoride substance (LiF 50% + BeF_2 50%) is selected for the filled rotor concept. No benefit is found from the temperature or the friction and wear data with the present configuration.

REFERENCES

1. T.L. Ho and M.B. Peterson, "Development of Aircraft Brake Materials," NASA CR-134663, March 1974.
2. J.J. Santani, "Effect of Design Factors on Surface Temperature and Wear in Disk Brakes," Project Technical Report (submitted for approval as NASA CR).
3. F.E. Kennedy, Jr., J.J. Wu and F.F. Ling, "A Thermal, Thermoelastic and Wear Analysis of High-Energy Disk Brakes," NASA CR-134507, January 1974.
4. T.L. Ho, F.E. Kennedy, Jr. and M.B. Peterson, "Evaluation of Materials and Design Modifications for Aircraft Brakes," NASA CR-134896, January 1975.
5. M.B. Peterson and T.L. Ho, "Consideration of Material for Aircraft Brakes," NASA CR-121116, April 1972.
6. C.J. Smithells, Metals Reference Book, 3rd, Butterworths, 1962.
7. Chemical Rubber Company, Handbook of Tables for Applied Engineering Science, The Chemical Rubber Company, 1970.
8. Y.S. Touloukian, "Thermophysical Properties of High Temperature Solid Materials," Vols.I and II, MacMillan Co., 1967.
9. E.M. Levin, "Phase Diagrams for Cermists," American Ceramic Society, 1964.
10. H.S. Carslaw and J.C. Jaeger, Conduction of Heat in Solids, Oxford University Press, 1959.
11. G.W. Evans, E. Isaacson and J.K.L. MacDonald, "Stefan-Like Problems," Quarterly of Applied Mathematics, Vol.III, No.3, 1949.

APPENDIX I

1. Determination of a Conservative Estimate of the Heat Capacity [C = Heat Capacity]

Although heat capacity is not constant, in general its value is lowest for the solid phase. The heat capacity was evaluated at 298°K and this will yield a conservative value for C. The expression for C is:

$$C = a + b(10^{-3})\ T + c(10^{-5})\ T^{-2}$$

where a and b are approximately the same order of magnitude and c = .1 for all the substances listed. The worst case of any substance considered was when a = b C = .1. Then C(at 298°K) = .242 and C (at 933°K) = .205 which is an error of less than 20%. Therefore assuming the heat capacity to be constant at 298°K will not yield any misleading information in Table I.

2. Calculation of Heat of Fusion of Alloys [H_f = Heat of Fusion]

In the calculation of the heat of fusion of alloys, if the intermetallic phase is completely disordered then H_f/T_{melt} can be calculated additively from the H_f/T_{melt} of the individual constituents. However, if completely ordered then a factor of $-4.573\ (N_1 \log N_1 + N_2 \log N_2)$ should be added to the H_f/T_{melt}. The term to be added is positive because both N_1 and N_2 are less than 1. A conservative estimate of H_f/T_{melt} is desired and therefore the H_f/T_{melt} was calculated assuming a completely disordered metallic phase, yielding conservative (smaller values of H_f. For a more complete discussion, see Ref.5.

3. Calculation of the Densities of Alloys

The densities of the alloys were obtained by taking the percentage by weight of the densities of the alloying components.

APPENDIX II

The Derivation of an Approximate Expression for the Motion of the Solid-Liquid Boundary within the Rotor (Ref.10)

Each stator is sandwiched between two rotors and each rotor applies a constant loading to the stator. Because of the symmetry of the problem it can be reduced to a disk of half the thickness with a uniform heat flux Q on one surface and insulated on the other major surface.

Simplifications

1) Since the conductivity of the steel encasing material is so much larger than the conductivity of the fluoride, only the temperature characteristics of the fluoride block during melting was modeled.
2) The block has been assumed to be semi-infinite in the direction of heat flow and infinite in the other directions.
3) Uniform constant heat source on the face of the slab. Thus, the problem will involve only one space dimension.
4) The coefficient of thermal diffusivity is assumed to be constant.

The object is to find the propagation of the liquid-solid interface through the slab. To determine the type of discontinuity across the interface, assume that the recrystallization has already occurred to a distance X where $0 < X < \infty$. The subscript 1 after a symbol will be used to indicate the solid region and the subscript 2 to indicate the liquid region.

Define

U_2 = Adjusted temperature in liquid region $T_2 - T_{melting}$
U_1 = Adjusted temperature in solid region $T_1 - T_{melting}$
ρ = Density
H_f = Heat of fusion
K_1 = Thermal conductivity of the solid
K_2 = Thermal conductivity of the liquid
Q = Heat flux into the surface
$X(t)$ = Location of the solid-liquid boundary
$\Phi(x)$ = Initial temperature distribution in the solid fluoride region minus the melting point temperature
g = Adjusted heat flux = $-Q/K_2$
α = Diffusivity of the solid

$\Phi(x)$ is assumed to be expressible in a Taylor series expansion about $x = 0$ with an infinite radius of convergence

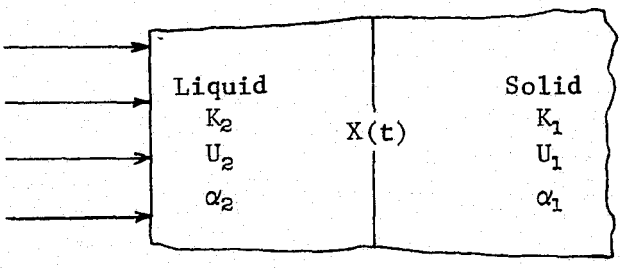

The heat balance across the interface is

$$\rho_1 H_f X(t) = K_2 \left.\frac{\partial U_2}{\partial x}\right|_{x=X(t)} - K_1 \left.\frac{\partial U_1}{\partial x}\right|_{x=X(t)} \tag{1a}$$

Additional boundary conditions are:

$$X(t = 0) = 0 \tag{1b}$$

$$U_1(x, 0) = \Phi(x) \tag{1c}$$

$$\frac{\partial U_2}{\partial x}(0, t) = g \tag{1d}$$

The temperature distribution in the liquid region is:

$$\frac{\partial U_2}{\partial t} = \alpha_2^2 \frac{\partial^2 U_2}{\partial x^2} \quad \text{for} \quad 0 < x < X(t) \tag{2}$$

The temperature distribution in the solid region is:

$$\frac{\partial U_1}{\partial t} = \alpha_1^2 \frac{\partial^2 U_2}{\partial x^2} \quad \text{for} \quad X(t) < x < \infty \tag{3}$$

The temperature distribution at the interface is:

$$U_1(X(t), t) = U_2(X(t), t) = 0 \tag{4}$$

It is possible to obtain a power series representation for $X(t)$ about $t = 0$, by assuming $U(x,t)$ expressible in a power series about $x = 0$, $t = 0$ for all U in the region $0 \leq x \leq X(t)$. Any discontinuities in the derivatives of U are assumed to occur only on crossing the $X(t)$ boundary.

Assume

$$X(t) = \sum_{n=0}^{\infty} C_n t^n \tag{5}$$

$$U_1(x,t) = \sum_{i,j=0}^{\infty} a_{ij} x^i t^j \tag{6}$$

$$U_2(x,t) = \sum_{i,j=0}^{\infty} b_{ij} x^i t^j \tag{7}$$

where a_{ij}, b_{ij} and C_n are coefficients to be determined.

Equations (5), (6), (7) can be differentiated to yield:

$$X(t) = \sum_{n=0}^{\infty} C_{n+1}(n+1)t^n \tag{8}$$

$$U_{1x} = \sum_{i,j=0}^{\infty} a_{i+1,j}\,(i+1)x^i t^j \tag{9}$$

$$U_{1xx} = \sum_{i,j=0}^{\infty} a_{i+2,j}\,(i+1)(i+2)x^i t^j \tag{10}$$

$$U_{1t} = \sum_{i,j=0}^{\infty} a_{i,j+1}(j+1)x^i t^j \tag{11}$$

$$U_{2x} = \sum_{i,j=0}^{\infty} b_{i+1,j}(i+1)x^i t^j \tag{12}$$

$$U_{2xx} = \sum_{i,j=0}^{\infty} b_{i+2,j}(i+1)(i+2)x^i t^j \tag{13}$$

$$U_{2t} = \sum_{i,j=0}^{\infty} b_{i,j+1}(j+1)x^i t^j \tag{14}$$

Equations (1b) and (5) yield $C_0 = 0$, Eqs.(1d) and (7) yield $b_{10} = g$. Substituting Eqs.(5), (8), (9) and (10) into Eq.(1a) yields the following recurrence relation

$$\sum_{i,j=0}^{\infty} (i+1)(K_2 b_{i+1,j} - K_1 a_{i+1,j})\Big(\sum_{m=0}^{\infty} C_m t^m\Big)^i t^j = \rho H_f \sum_{n=0}^{\infty} (n+1)C_{n+1} t^n \tag{R1}$$

Substituting Eqs.(5,6) into Eq.(4) yields

$$\sum_{i,j=0}^{\infty} a_{i,j}\left(\sum_{n=0}^{\infty} C_n t^n\right)^i t^j = 0 \qquad \text{(R2)}$$

Substituting Eqs.(5,7) into Eq.(4) yields

$$\sum_{i,j=0}^{\infty} b_{i,j}\left(\sum_{n=0}^{\infty} C_n t^n\right)^i t^j = 0 \qquad \text{(R3)}$$

Substituting Eqs.(13) and (14) into Eq.(2) and rearranging yields

$$b_{i+2,j} = \frac{(j+1)}{\alpha_2^2 (i+1)(i+2)}\, b_{i,j+1} \qquad \text{(R4)}$$

Substituting Eqs.(10) and (11) into Eq.(3) and rearranging yields

$$a_{i+2,j} = \frac{(j+1)}{\alpha_1^2 (i+1)(i+2)}\, a_{i,j+1} \qquad \text{(R5)}$$

The five resulting equations [(R1), (R2), (R3), (R4), (R5)], can be solved for the coefficients $a_{i,j}$, $b_{i,j}$ and C_n. The series representing X(t), (the movement of the solid-liquid boundary with time), is given below (through the second power of t).

$$X(t) = \frac{1}{\rho H_f}\left[K_2 g - K_1 \Phi'(0)\right]t + \frac{1}{2\rho H_f}\left[K_2\left[\frac{-g}{\alpha_2^2 \beta^2}\left(K_2 g - K_1 \Phi'(0)\right)^2\right] - K_1\left[\frac{\Phi''(0)}{\rho H_f}\left(K_2 g - K_1 \Phi'(0)\right) + \alpha_1^2\, \Phi''(0)\right]\right]t^2 . \qquad (15)$$

This expression can be used to obtain the location of the solid-liquid boundary, but first the initial temperature distribution of the solid fluoride mixture (when the surface is at the melting point), must be found and expressed in a Taylor series expansion around x = 0.

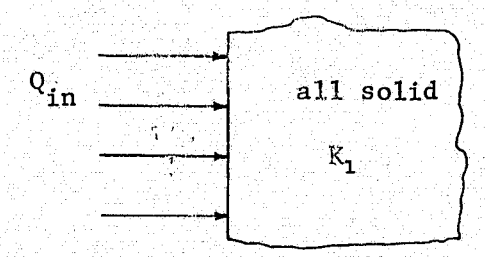

Let W be temperature defined as $W = T - T_{initial}$, then the initial condition becomes: $W(t=0) = 0$, and if Q is the heat flux into the material it has been shown by Carslaw and Jaeger (Ref.9) that the temperature distribution is

$$W = \frac{2Q}{K_1}\left[\left(\frac{\alpha t}{\pi}\right)^{\frac{1}{2}} e^{-(x^2/4\alpha t)} - \frac{X}{2}\,\mathrm{erfc}\left(\frac{X}{2\sqrt{\alpha t}}\right)\right] \tag{16}$$

or

$$W = \frac{Q}{K_1}\int_x^\infty \mathrm{erfc}\left(\frac{X}{2\sqrt{\alpha t}}\right) dX \tag{17}$$

The time (t_m), for the surface to reach the melting temperature (T_{melt}, that is at time t_m is simply

$$T_{melt} - T_{initial} = \frac{2Q}{K_1}\left(\frac{\alpha t}{\pi}\right)^{\frac{1}{2}} \tag{18}$$

which reduces to

$$t_m = \frac{\pi K_1^2 (T_{melt} - T_{initial})^2}{4Q^2\alpha} \tag{19}$$

The temperature distribution when the surface is at T_{melt}, that is at time t_m is simply

$$\Phi(X) = W\Big|_{\substack{At\\ t_m}} = T_{initial} - T_{melt} + (Q/K_1)\int_x^\infty \mathrm{erfc}\left(\frac{X}{2\sqrt{\alpha t_m}}\right) dX \tag{20}$$

$$\Phi(X) = T_{initial} - T_{melt} + \left(\frac{2Q}{K_1}\right)\left[\left(\frac{\alpha t_m}{\pi}\right)^{\frac{1}{2}} e^{-(x^2/4\alpha t_m)} - \frac{X}{2}\,\mathrm{erfc}\left(\frac{X}{2\sqrt{\alpha t_m}}\right)\right] \tag{21}$$

This can now be expressed as a Taylor series expansion

$$\Phi(x) = -(Q/K_1)X + \frac{1}{\sqrt{\pi}}(Q/K_1)X^2 - (Q/K_1)\frac{1}{4!(\sqrt{\pi}\,\alpha t_m)}X^4 + \ldots. \tag{22}$$

The propagation of the solid-liquid boundary can now be investigated. However, the thermal conductivity of the LiF-BeF_2 mixture in the solid and liquid phase is unknown! In fact many thermophysical properties of salts or salt eutectics are unknown.

Since it is desired to determine approximately how large a quantity of $LiF\text{-}BeF_2$ could be completely melted during a normal braking, a very conservative K value is assumed in performing the calculations.

To estimate the thermal conductivity, a weighted average of the components is taken and half this value as a conservative estimate of the conductivity of both solid and liquid phases is used.

This procedure yields: $K_{solid} = .0261$ (cal/(sec cm °F)) and $K_{liquid} = .00261$ (cal/(sec cm^2 °F)).

During a normal stop, a 90(cal/(sec cm^2)) average heat flux is generated, and thus a conservative expression for the location of the liquid solid boundary X(t), is (from Eq.(15))

$$X(t) = .257\ t + .00268\ t^2 \qquad (23)$$

A normal stop takes 20 seconds and X(t 20) = 6.20 cm = 2.44", which means the brake must have a half width of less than approximately 2.44". The proposed design calls for a half width of .375" and since the quantity that is capable of being melted during a normal stop far exceeds the amount of fluoride in this design, the assumed conservative value of K was not critical.

In summary, for the design proposed, no problem with the thermal conductivity of the fluoride, or with its complete melting is to be expected.

APPENDIX III

Calculation of Apparent Pressure of Contact (N/m^2), PV (N/m^2-sec), and the Frictional Kinetic Energy (Joules)

1. Calculation of Apparent Pressure of Contact (N/m^2)

Let: A_p - area of one pad

A_T - total area of the frictional pads on a stator

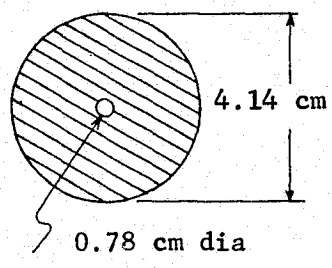

$$A_p = \frac{\pi}{4}(D_{out}^2 - D_{in}^2)$$

$$A_p = \frac{\pi}{4}(4.14^2 - .78^2)[cm^2] = 12.98 \times 10^{-4}[m^2/pad]$$

$$A_T = (12[pads/stator])(12.98 \times 10^{-4}[m^2/pad])$$

$$A_T = .01558\ m^2$$

$$\text{Applied Force} = \text{Pair}\left[\frac{lb_f}{in^2}\right]\left(\frac{.4536\ kg}{lb_f}\right)\left(\frac{9.81\ m}{sec^2}\right)(8.1\ in^2)$$

$$\text{Applied Force (Newtons)} = \text{Pair[psi]} \times 36.04\left[\frac{\text{Newtons}}{\text{psi}}\right]$$

$$\text{Apparent Pressure} = \frac{\text{Applied Force}}{A_T} = \frac{\text{Pair[psi]} \times \left[\frac{\text{Newtons}}{\text{psi}}\right]}{.01558\ [m^2]}$$

$$\text{Apparent Pressure}[\text{Newtons}/m^2] = \text{Pair [psi]} \times \left(2.313 \times 10^3\left[\frac{\text{Newtons}}{m^2\ \text{psi}}\right]\right)$$

2. Calculation of PV (N/m^2-sec)

$$PV = (\text{Apparent Pressure } [N/m^2])\left(W\left[\frac{rad}{sec}\right]\right)$$

$$PV = (\text{Pair [psi]})(R[rpm])\left(2.423 \times 10^2\left[\frac{N}{m^2 - sec} \cdot \frac{1}{rpm - psi}\right]\right)$$

3. Calculation of Kinetic Energy (Joules)

$$KE = \int \tau\omega \, dt \approx \sum_{i=1}^{n} \tau_i \omega_i \, \Delta T$$

$$KE \approx \left(.142\left[\frac{\text{Joules}}{\text{ft-lb}_f\text{-rpm-sec}}\right]\right) \times \sum_{i=1}^{n} \tau_i\,[\text{ft-lb}_f]\,W[\text{rpm}]\;\Delta T[\text{sec}]$$

A delta t of two seconds was used, yielding

$$KE \approx \left(.284\left[\frac{\text{Joules}}{\text{ft-lb}_f\text{-rpm}}\right]\right) \times \sum_{i=1}^{n} \tau_i\,[\text{ft-lb}_f]\;W_i\,[\text{rpm}]$$